Supporting Information

Single-Atom Fe-N_x-C Electrocatalysts for Efficient Nitrate Reduction Reaction

Simone Lombardi,[1] Lucia Codega[1], Mohsin Muhyuddin,[1] Nicola Lisi,[2] Valerio Ficca[2], Alessandro Lavacchi[3], Enrico Berretti,[3] Matteo Spotti[1], Giovanni Di Liberto[1], Francesco Paparoni[4], Javid Rezvani[5], *Rosanna Viscardi[2], **Carlo Santoro[1]

[1] Department of Materials Science, University of Milano-Bicocca, U5, Via Roberto Cozzi 55, 20125, Milano, Italy.
[2] Casaccia Research Center, ENEA, Department of Energy Technologies and Renewable Sources, Via Anguillarese 301, 00123, Santa Maria di Galeria, Rome, Italy.
[3] Istituto di Chimica Dei Composti OrganoMetallici (ICCOM), Consiglio Nazionale Delle Ricerche (CNR), Via Madonna Del Piano 10, 50019, Sesto Fiorentino, Firenze, Italy.
[4] Synchrotron SOLEIL, L'Orme des Merisiers,, 91190 Saint-Aubin, France.
[5] Physics Division, School of Science and Technology, University of Camerino, via madonna delle carceri 9, 62032 Camerino, MC, Italy.

Corresponding author:
* Dr. Rosanna Viscardi. rosanna.viscardi@enea.it
**Prof. Carlo Santoro. carlo.santoro@unimib.it

Section S1

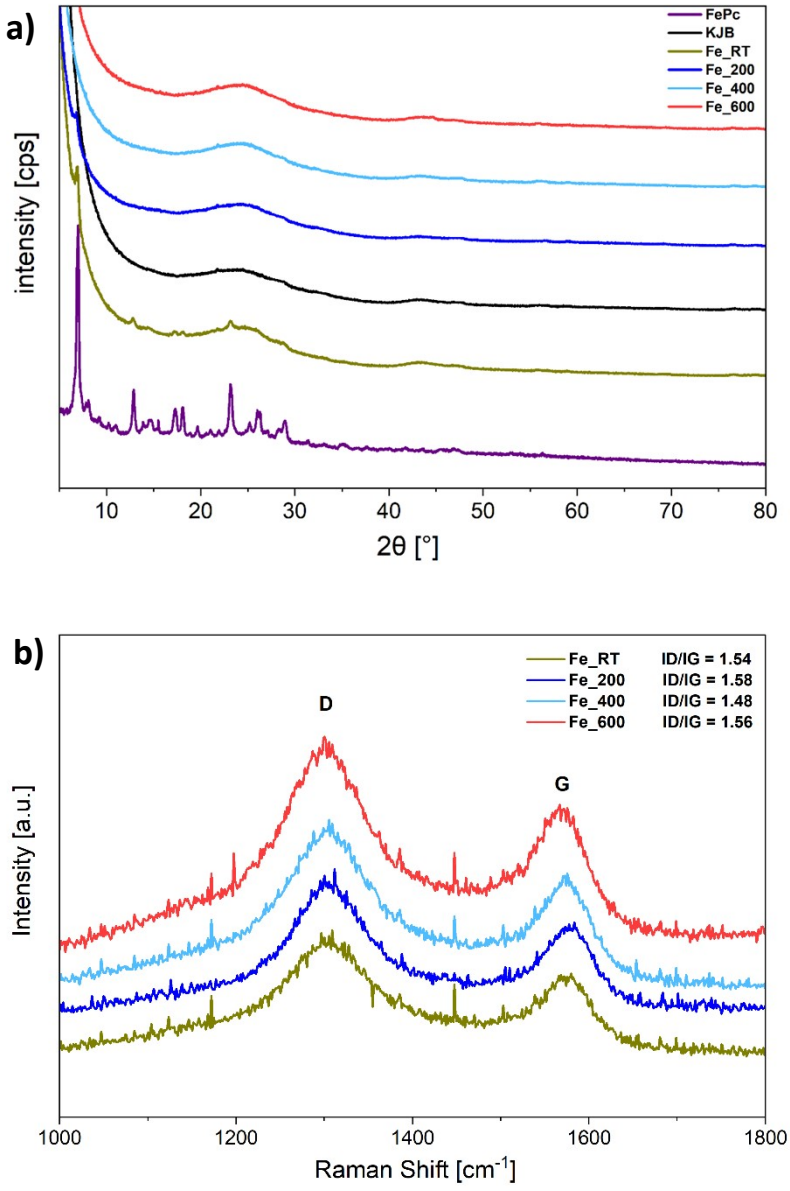

Figure S1. a) XRD pattern and b) Raman spectra of the different ECs.

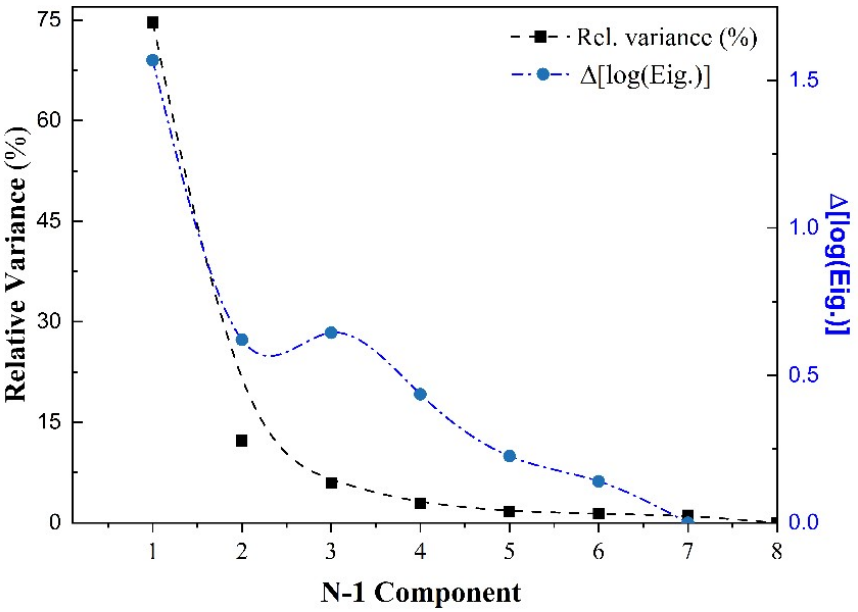

Figure S2. Principal Component Analysis (PCA) of the Fe K-edge XANES dataset. As suggested in the FASTOSH manual in the case of XANES spectra, the dataset was mean-centered prior to Singular Value Decomposition to mask the preponderant weight of the edge-jump. Hence, one degree of freedom is removed and the resulting factor space is described by N–1 components (where N is the number of spectra in the series); the horizontal axis is labelled accordingly. The black squares show the relative variance (%) explained by each successive component, while the blue circles show the difference in the logarithm of consecutive eigenvalues, Δ[log(Eig.)]. Both indicators exhibit a break/plateau after the fourth–fifth component, beyond which additional components contribute variance comparable to experimental noise. This indicates that 4–5 components are required to statistically account for the structured variance in the dataset.

Table S1. results of the target transformation analysis on a large dataset of candidate reference compounds, in the case of 4-component (left) and 5-component (right) models. Reference with unacceptable Malinowski SPOIL values (>6) were rejected. Comparing the SPOIL values obtained under the 4- and 5-component models shows a systematic improvement when moving to the 5-component model, indicating that a 4-component model is insufficient to properly resolve the oxide and metallic side-product references, which are only correctly embedded in the factor space once a fifth component is included. Notably, the sixth FeN_4 reference shows a SPOIL value of 4.8 in the 5-component model (between fair-poor boundary acceptability of the target transformation analysis) that does not exclude it may be a less well-resolved component of the mixture.

4-Component	SPOIL		5-Component	SPOIL
$(FePc)_2O$	2.6		**α-Fe_2O_3**	1.3
Fe_3O_4	3.3		**Fe_3O_4**	2
α-Fe_2O_3	3.3		**Fe**	3
FeN_4	3.7		**$(FePc)_2O$**	3.3
γ-Fe_2O_3	4.6		**FeN_3**	3.9
FeN_3	4.8		**FeN_4**	4.8

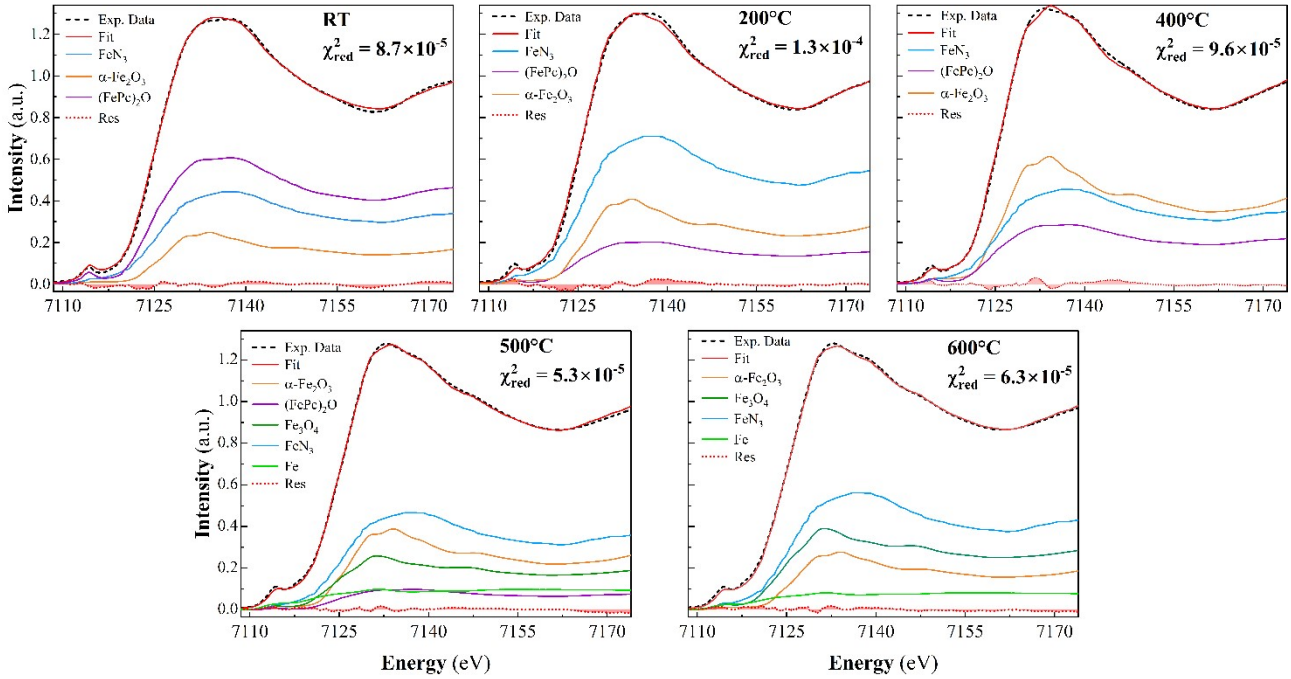

Figure S3. LCF with 5 components determined from Target transformation analysis.

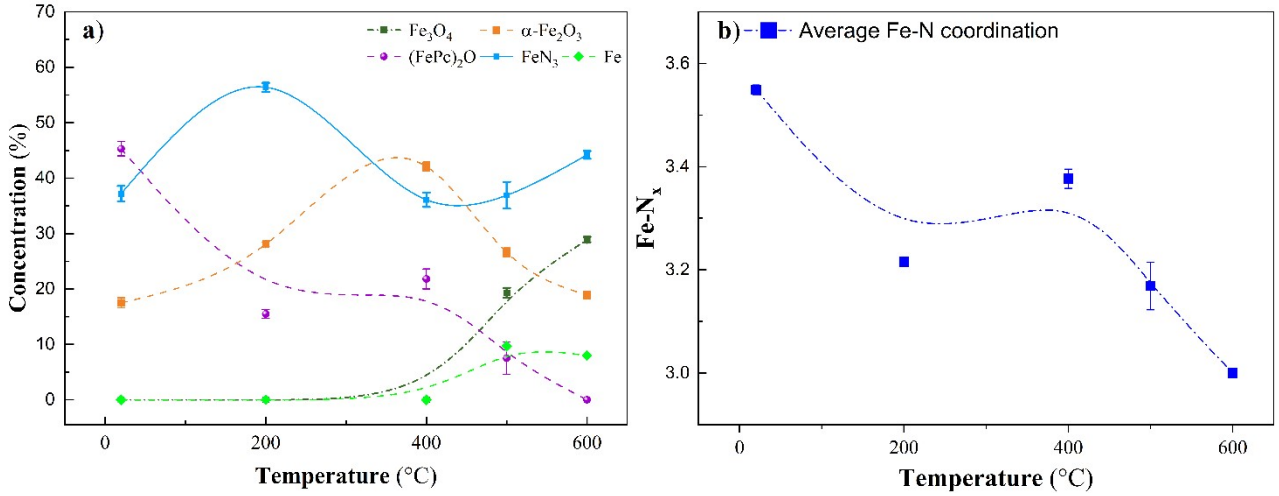

Figure S4. a) Species concentration estimated via 5-component LCF. b) Average N coordination estimated from the relative concentration of Fe-N_3 (x=3) and $(FePc)_2O$ (x=4). Errors are estimated as max variation between three fit iterations. The 5-component LCF yields the same species concentration vs. temperature behavior as the 6-component analysis given in the main text. Adding the 6th component improves fit precision but does not change the overall trend.

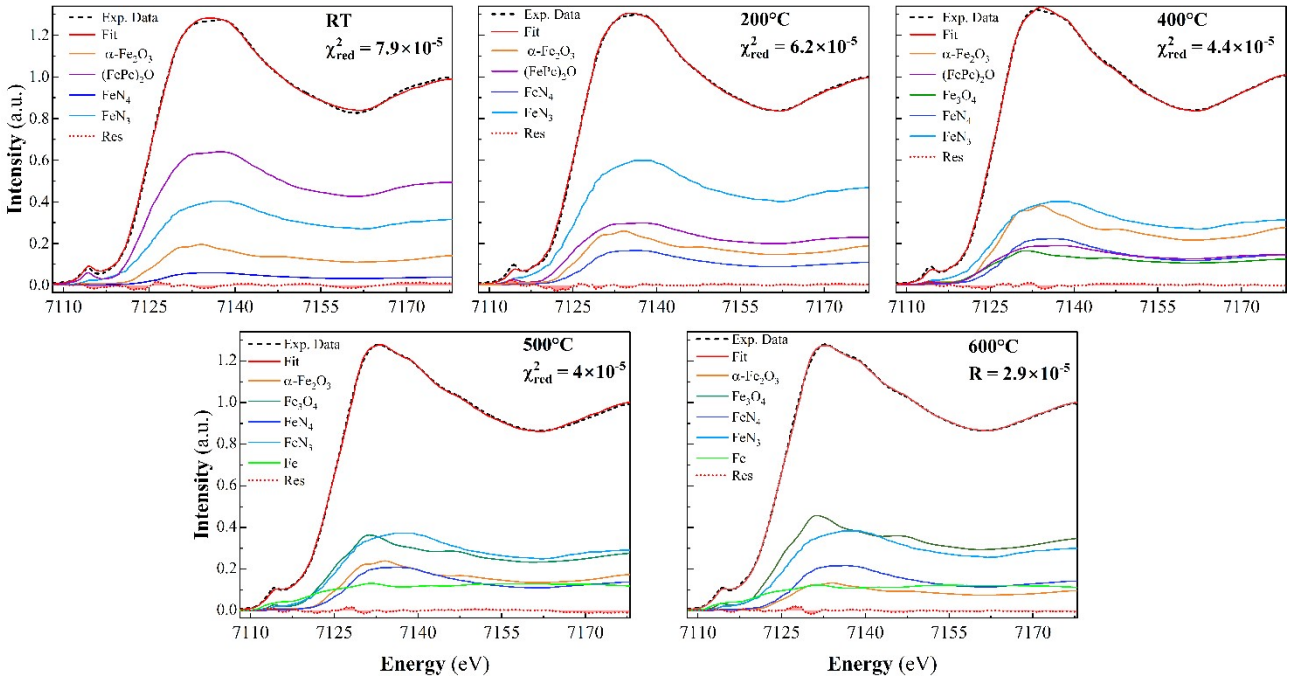

Figure S5. LCF with 6 components, as determined via Target Transformation analysis, including also the Fe-N_4 reference. Comparison of the reduced chi-square values confirm the improved agreement between the experimental and calculated spectra when adding the 6th component to the LCF.

Table S2. Results of LCF with 6 components

Sample	FeN_4	FeN_3	$(FePc)_2O$	Fe_2O_3	Fe_3O_4	Fe
Fe_RT	3.9±0.6	32.5±1.2	49.9±1.7	13.7±1.2	0	0
Fe_200	10.9±0.7	48.0±1.1	23.1±1.1	18.0±0.7	0	0
Fe_400	14.6±0.4	32.1±0.5	14.6±0.3	26.4±0.5	12.4±0.3	0
Fe_500	13.7±2	29.7±2.3	0	16.5±2.4	27.2±1.4	12.9±0.6
Fe_600	14.2±1.2	30.5±0.9	0	9.2±1	34.1±0.6	12.1±0.4

Table S3. Elemental composition of the different ECs determined by XPS

Sample	at.%				
	C1s	O1s	N1s	Fe2p	Cl2p
Fe_RT	95.9	3.5	0.6	0.0	0.0
Fe_100	98.3	1.2	0.5	0.0	0.0
Fe_200	94.2	3.3	2.1	0.3	0.0
Fe_300	93.8	3.5	2.4	0.3	0.0
Fe_400	94.7	2.2	2.6	0.5	0.0
Fe_500	86.6	11.1	2.2	0.2	0.0
Fe_600	95.2	2.7	1.8	0.3	0.0

Table S4. Chemical Speciation of identified elements determined by XPS

	Fe_RT		Fe_100		Fe_200		Fe_300		Fe_400		Fe_500		Fe_600	
Comp	**BE (eV)**	**rel.%**	**BE (eV)**	**rel.%**	**BE (eV)**	**rel.%**	**BE (eV)**	**rel.%**	**BE (eV)**	**rel.%**	**BE (eV)**	**rel.%**	**BE (eV)**	**rel.%**
C defect	283.8	3.9	283.8	3.6	283.8	3.7	283.9	4.2	283.9	4.1	283.9	3.9	283.9	4.2
C sp_2	284.4	64.1	284.4	67.3	284.4	62.5	284.4	61.0	284.4	63.7	284.4	58.2	284.5	62.7
C-C/C-H (sp_3)	285.0	11.9	285.0	9.8	285.0	12.1	285.0	11.7	285.0	11.2	285.0	14.3	285.0	11.4
C-O/C-N	285.6	8.7	285.7	6.7	285.6	9.4	285.6	10.6	285.6	9.2	285.6	11.9	285.6	9.4
C-O-C/C=N	286.5	4.7	286.6	4.5	286.5	5.3	286.5	4.9	286.6	4.9	286.6	5.8	286.5	5.1
C=O / amide	287.5	2.1	287.9	3.5	287.6	2.3	287.5	2.7	287.8	2.7	287.2	0.3	287.6	2.7
COOH	289.2	4.7	289.5	4.6	289.2	4.7	289.2	4.9	289.5	4.2	289.0	5.6	289.3	4.6
Sh-up	291.0	0.0	291.2	6.1	291.1	4.1	291.1	4.0	291.3	4.0	291.0	1.8	291.2	4.4
M-OH/C=O	531.0	4.8	530.4	15.2	530.7	5.4	530.8	9.3	530.6	7.8	530.3	2.9	530.6	2.9
C-OH/COC	532.3	50.7	531.7	49.5	532.2	50.1	532.2	48.4	532.2	49.5	532.2	50.5	532.3	49.2
OCO	533.6	44.6	533.1	35.3	533.6	44.5	533.5	42.3	533.6	42.6	533.7	46.6	533.7	47.9
H_2O ads	534.5	0.0	534.4	0.0	534.7	0.0	534.4	0.0	534.6	0.0	535.0	0.0	534.9	0.0
Imine / cyano	398	0	398	0	398	0	397.4	0.8	397.8	1.0	397.7	1.8	397.5	2.2
Aza-N/pyridinic N	398.7	41.8	398.6	44	398.7	41.8	398.6	53.0	398.7	72.2	398.6	67.0	398.7	74.0
Nx-Fe / amine	399.7	37.8	399.8	38.8	399.7	37.8	399.6	26.8	399.7	17.1	399.5	16.8	400.0	14.9
N-H (pyrrolic)	400.5	20.4	400.6	17.2	400.5	20.4	400.5	19.4	400.6	9.6	400.4	14.3	400.9	8.9
Fe-Nx/Fe(II)	0.0	-	0.0	-	709.1	62.4	709.6	54.4	709.3	64.5	709.3	62.5	709.3	64.5
Fe(III)	0.0	-	0.0	-	711.5	37.6	711.6	45.6	711.6	35.5	711.9	37.5	711.6	35.5
sat (II)	0.0	-	0.0	-	714.5	0.0	714.7	0.0	714.5	0.0	714.5	0.0	714.5	0.0
sat (III)	0.0	-	0.0	-	718.7	0.0	719.0	0.0	718.3	0.0	718.4	0.0	718.7	0.0

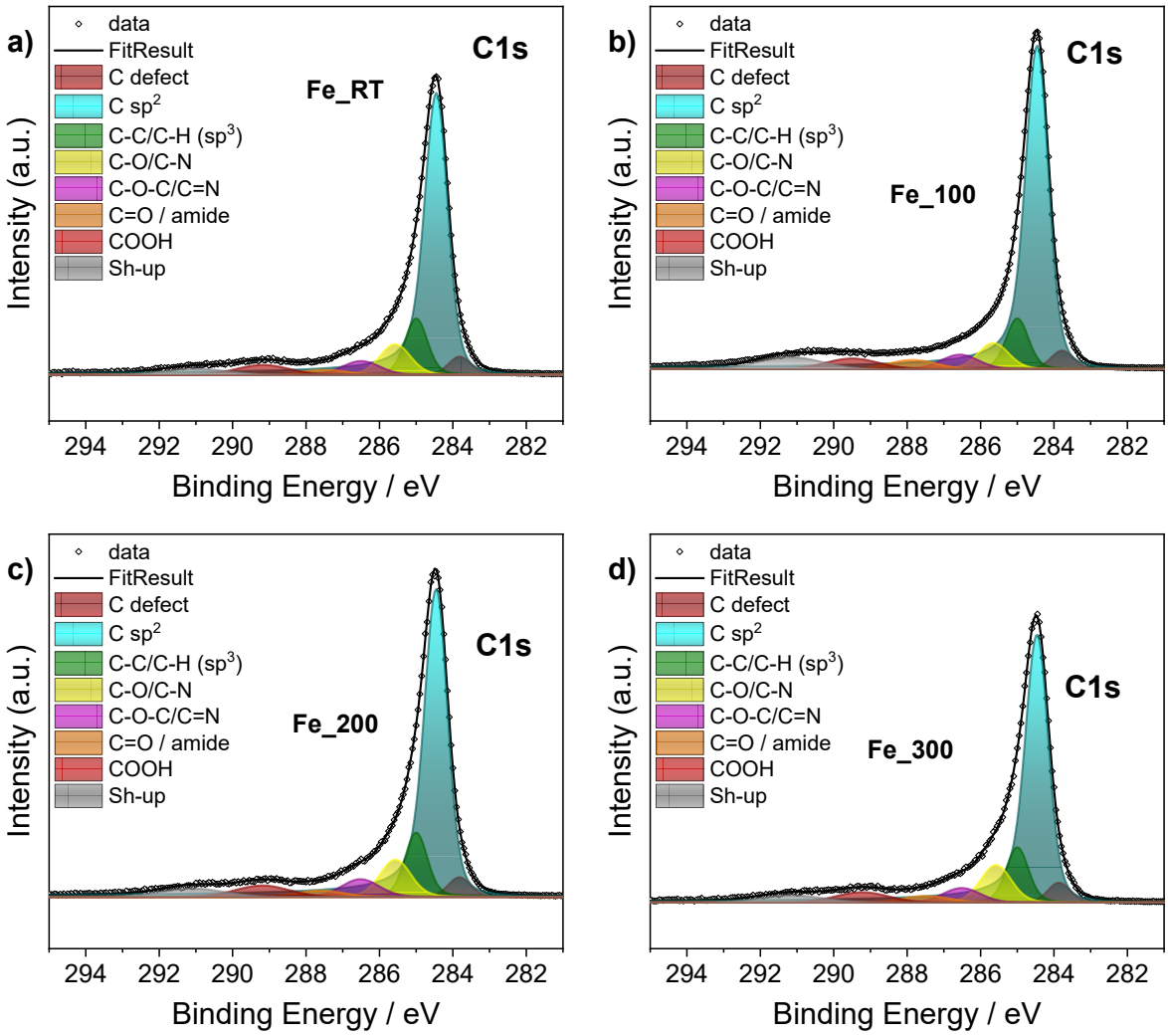
a)
b)
c)
d)
data
FitResult
C defect
C sp2
C-C/C-H (sp3)
C-O/C-N
C-O-C/C=N
C=O / amide
COOH
Sh-up
C1s
Fe_RT
Fe_100
Fe_200
Fe_300
Intensity (a.u.)
Binding Energy / eV
294
292
290
288
286
284
282

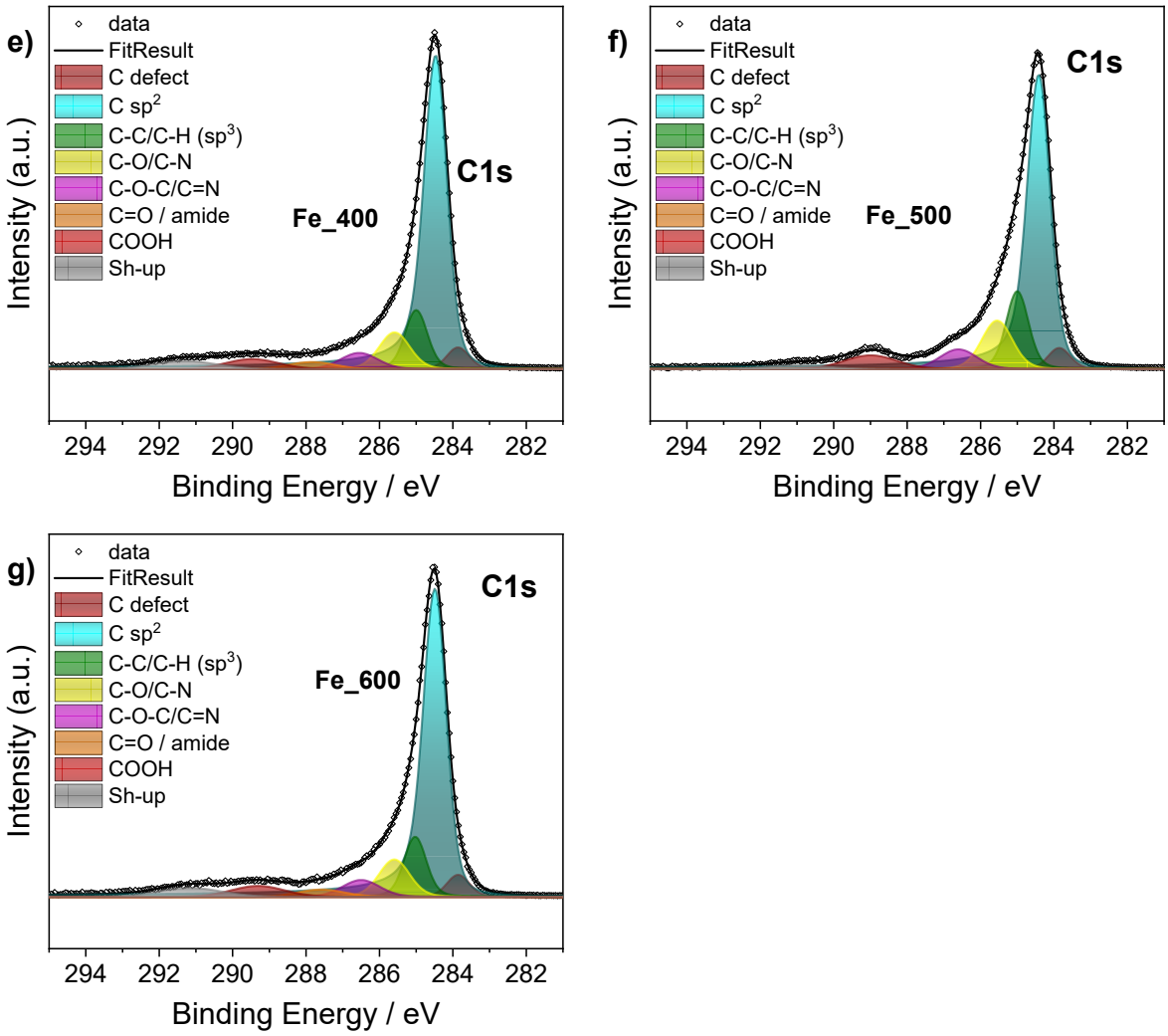

Figure S6. C1s core levels and corresponding deconvolution of a) Fe_RT, b) Fe_100, c) Fe_200, d) Fe_300, e) Fe_400, f) Fe_500 and g) Fe_600

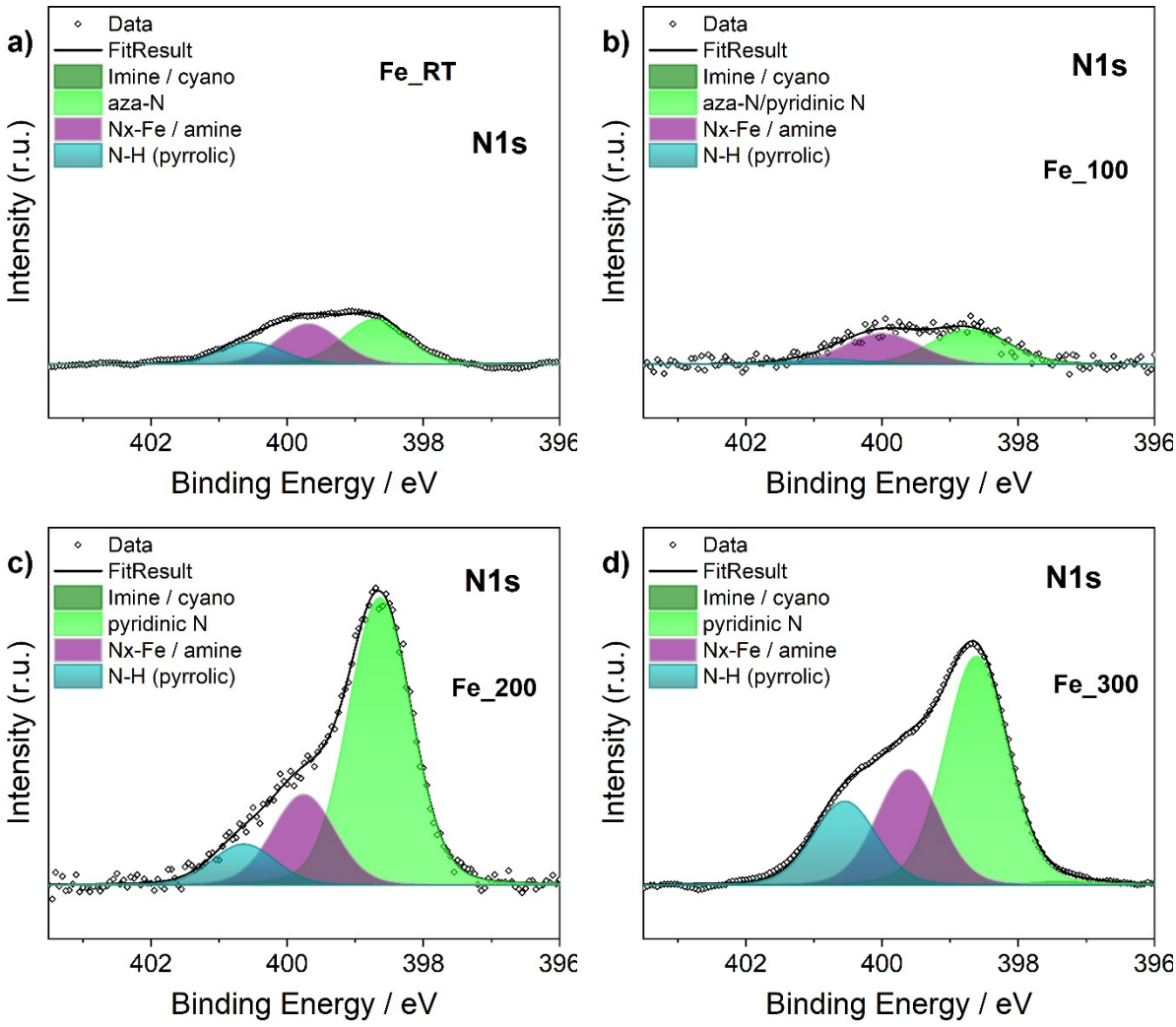
a)
Data
FitResult
Imine / cyano
aza-N
Nx-Fe / amine
N-H (pyrrolic)
Fe_RT
N1s
Intensity (r.u.)
402
400
398
396
Binding Energy / eV
b)
Data
FitResult
Imine / cyano
aza-N/pyridinic N
Nx-Fe / amine
N-H (pyrrolic)
N1s
Fe_100
Intensity (r.u.)
402
400
398
396
Binding Energy / eV
c)
Data
FitResult
Imine / cyano
pyridinic N
Nx-Fe / amine
N-H (pyrrolic)
N1s
Fe_200
Intensity (r.u.)
402
400
398
396
Binding Energy / eV
d)
Data
FitResult
Imine / cyano
pyridinic N
Nx-Fe / amine
N-H (pyrrolic)
N1s
Fe_300
Intensity (r.u.)
402
400
398
396
Binding Energy / eV

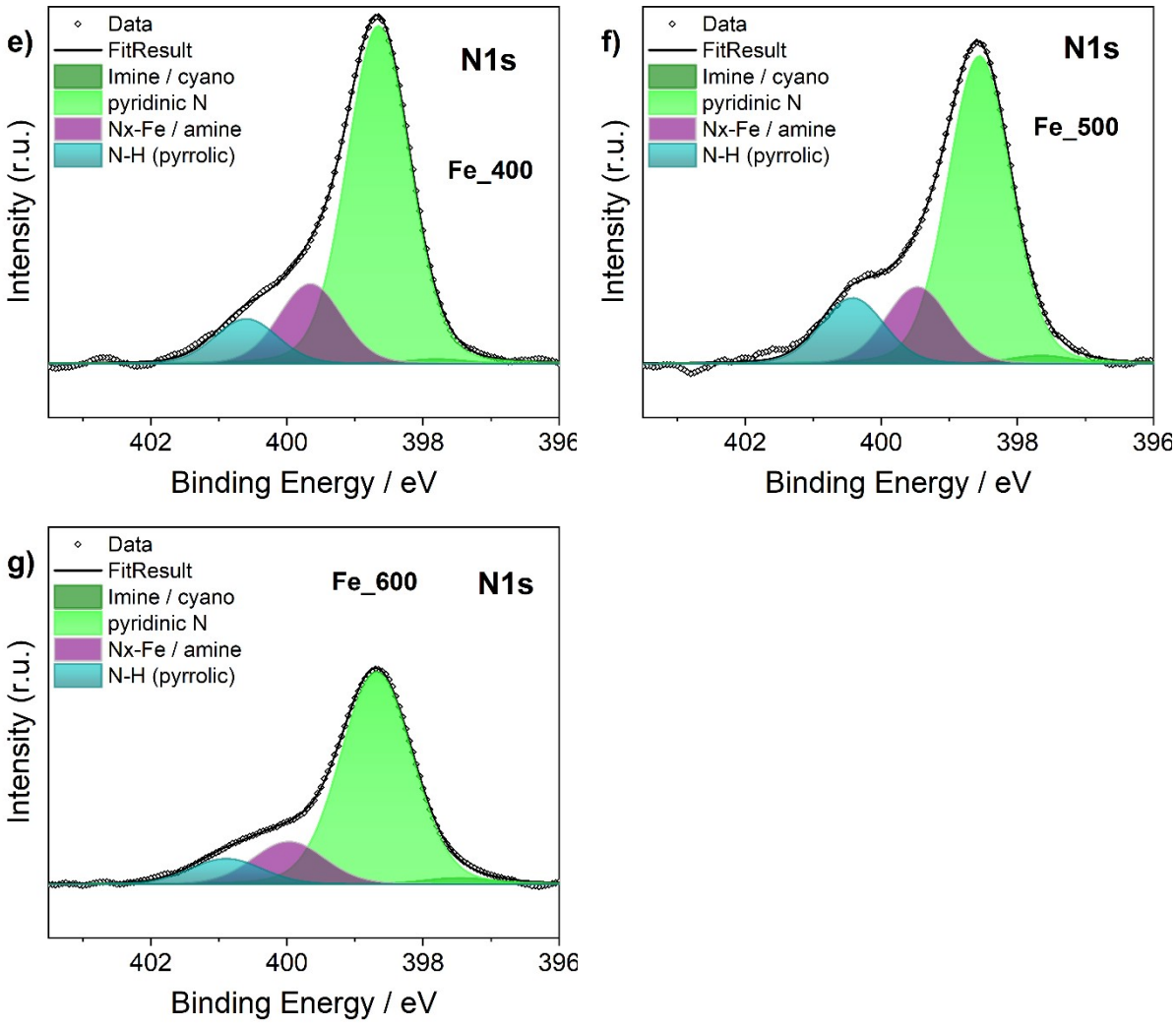

Figure S7. N1s core levels and corresponding deconvolution of a) Fe_RT, b) Fe_100, c) Fe_200, d) Fe_300, e) Fe_400, f) Fe_500 and g) Fe_600

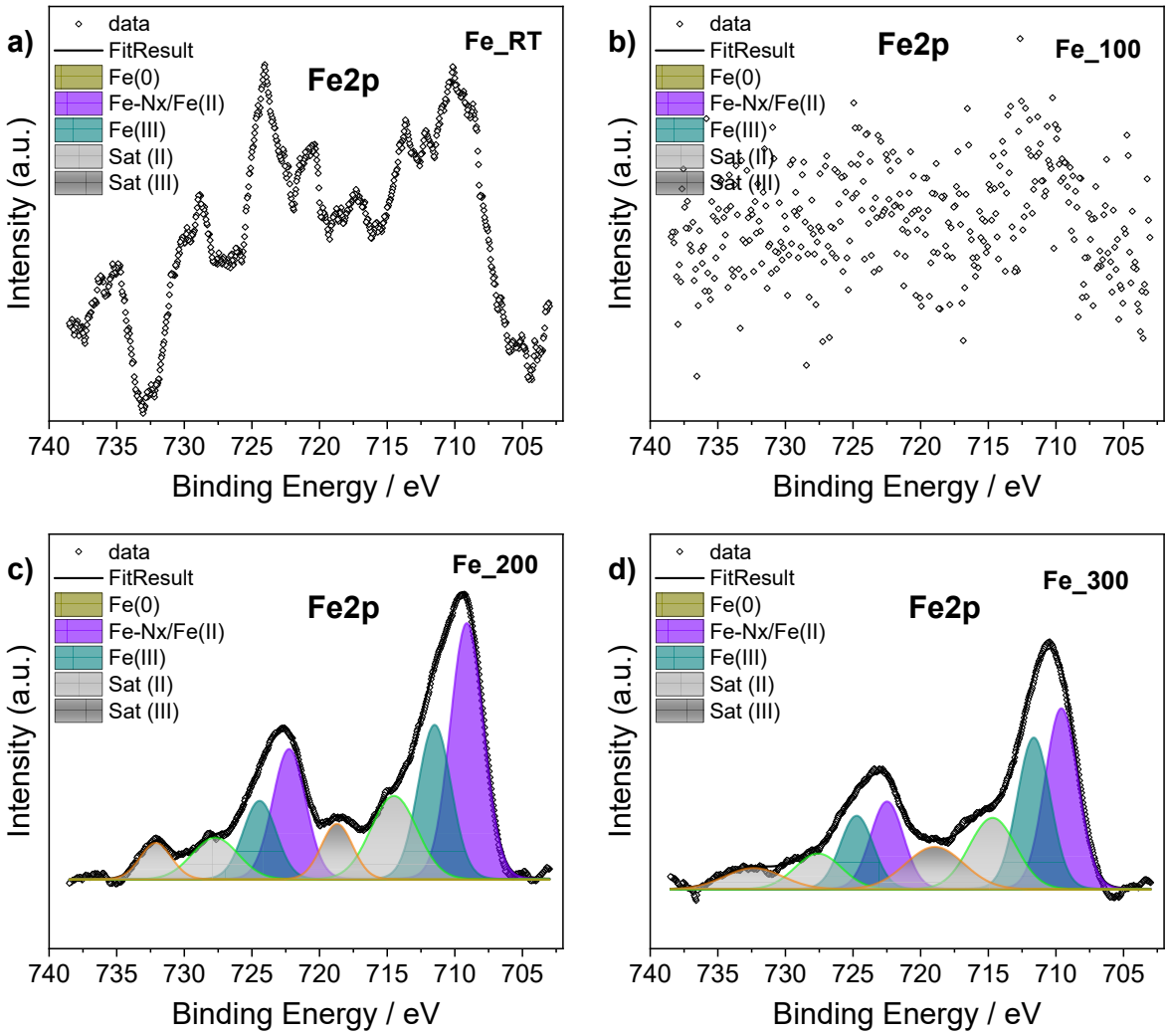
a)
Fe_RT
Fe2p
data
FitResult
Fe(0)
Fe-Nx/Fe(II)
Fe(III)
Sat (II)
Sat (III)
Intensity (a.u.)
740 735 730 725 720 715 710 705
Binding Energy / eV
b)
Fe_100
Fe2p
c)
Fe_200
Fe2p
d)
Fe_300
Fe2p

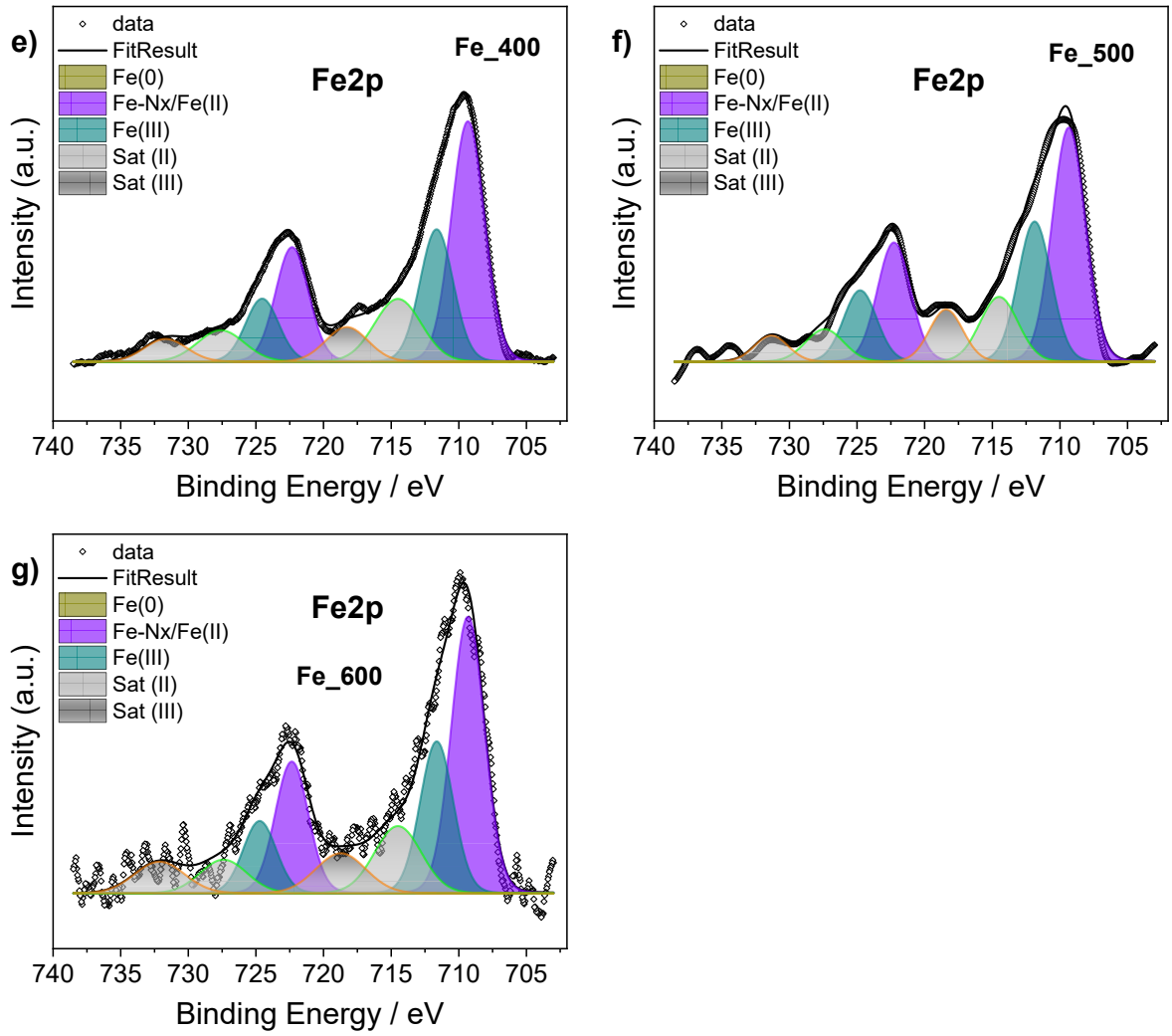

Figure S8. Fe2p core levels and corresponding deconvolution of a) Fe_RT, b) Fe_100, c) Fe_200, d) Fe_300, e) Fe_400, f) Fe_500 and g) Fe_600. Fe_RT and Fe_ 100 resulted in lower N content due to instability of the non-pyrolyzed FePc complex in ultra high vacuum.

Table S5**.** Onset potentials of each EC for NO_3RR derived from the LSV data, defined as the potential at which a current density of -0.4 mA cm^{-2} is reached.

Sample	E Onset (V. vs RHE)
Fe_rt	-0.46 ± 0.04
Fe_100	-0.49 ± 0.03
Fe_200	-0.47 ± 0.03
Fe_300	-0.45 ± 0.05
Fe_400	-0.46 ± 0.04
Fe_500	-0.44 ± 0.01
Fe_600	-0.43 ± 0.02

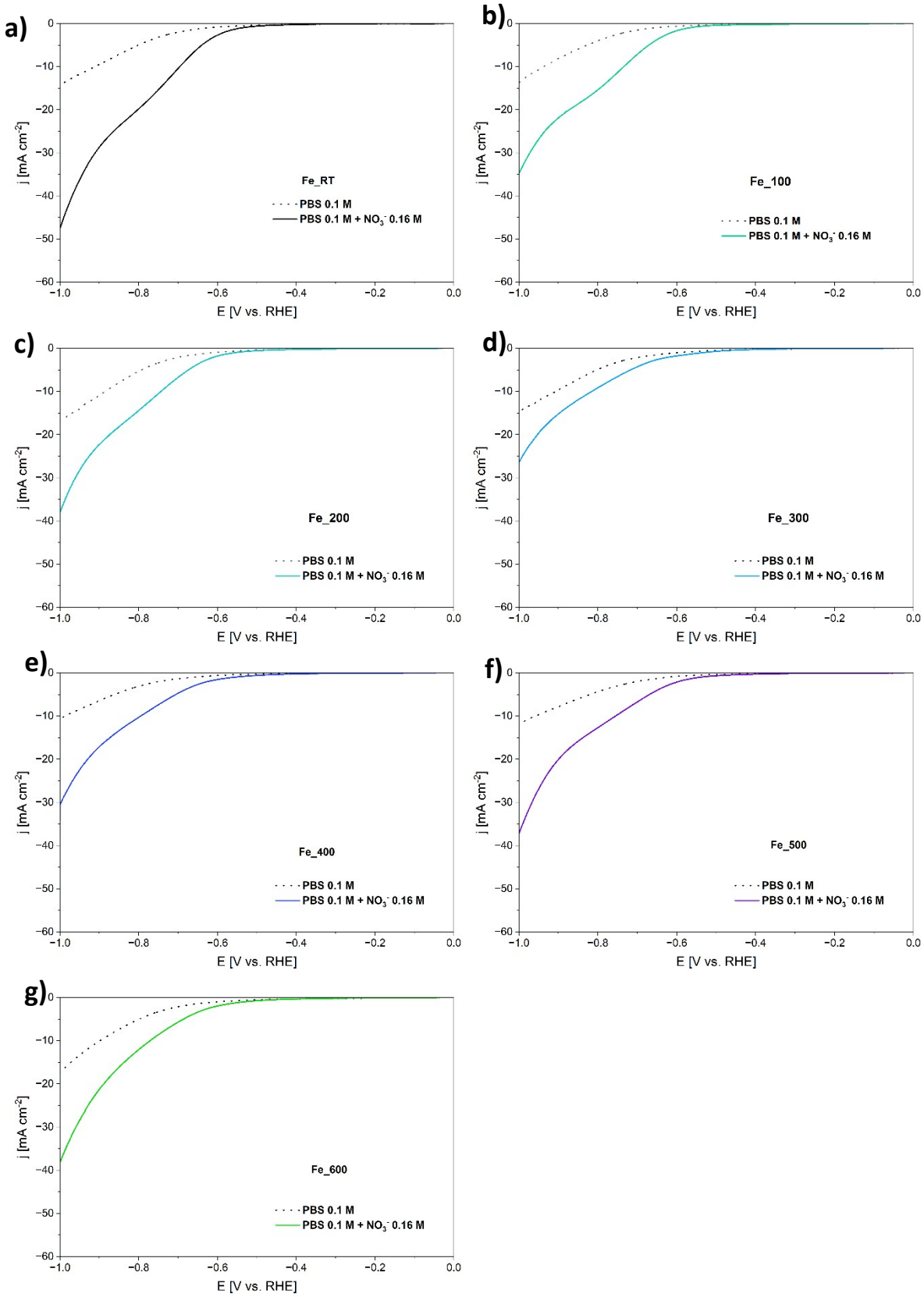

Figure S9. LSV curves for a) Fe_RT, b) Fe_100, c) Fe_200, d) Fe_300, e) Fe_400, f) Fe_500 and Fe_600 in 0.1 M PBS (dotted line), and in 0.1 M PBS + 0.16 M NO_3^- (solid line).

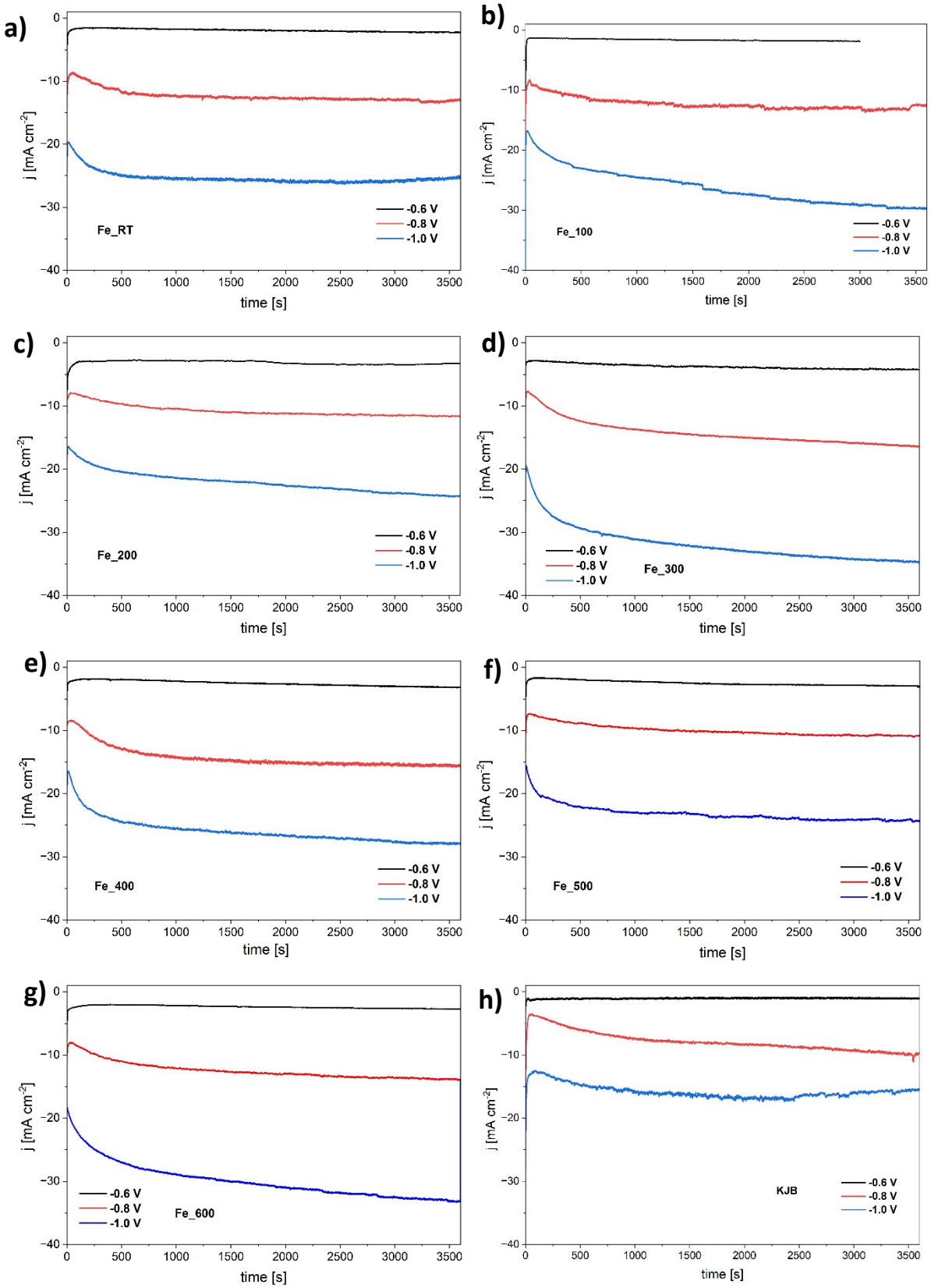

Figure S10. NO_3RR chronoamperometry tests over a a) Fe_RT, b) Fe_100, c) Fe_200, d) Fe_300, e) Fe_400, f) Fe_500, g) Fe_600 and h) KJB. NO_3RR electrolysis is performed for 1 h in a 0.1M PBS + 0.16M NO_3^- electrolyte, at applied potentials of -1.0 V (blue), -0.8 V (red) and -0.6 V (black) vs. RHE, respectively.

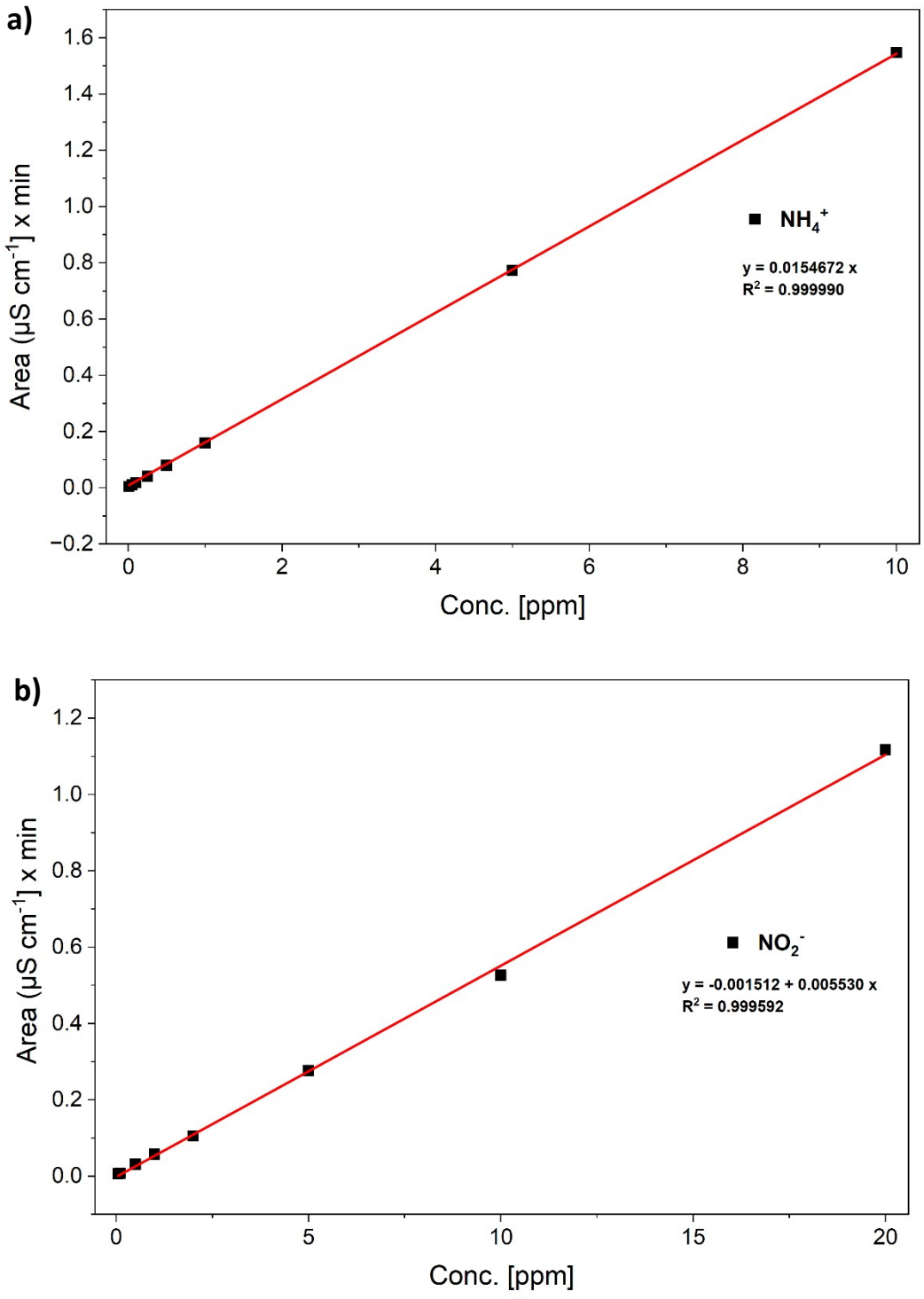

Figure S11. IC calibration curves used for quantification of a) NH_4^+ and b) NO_2^-.

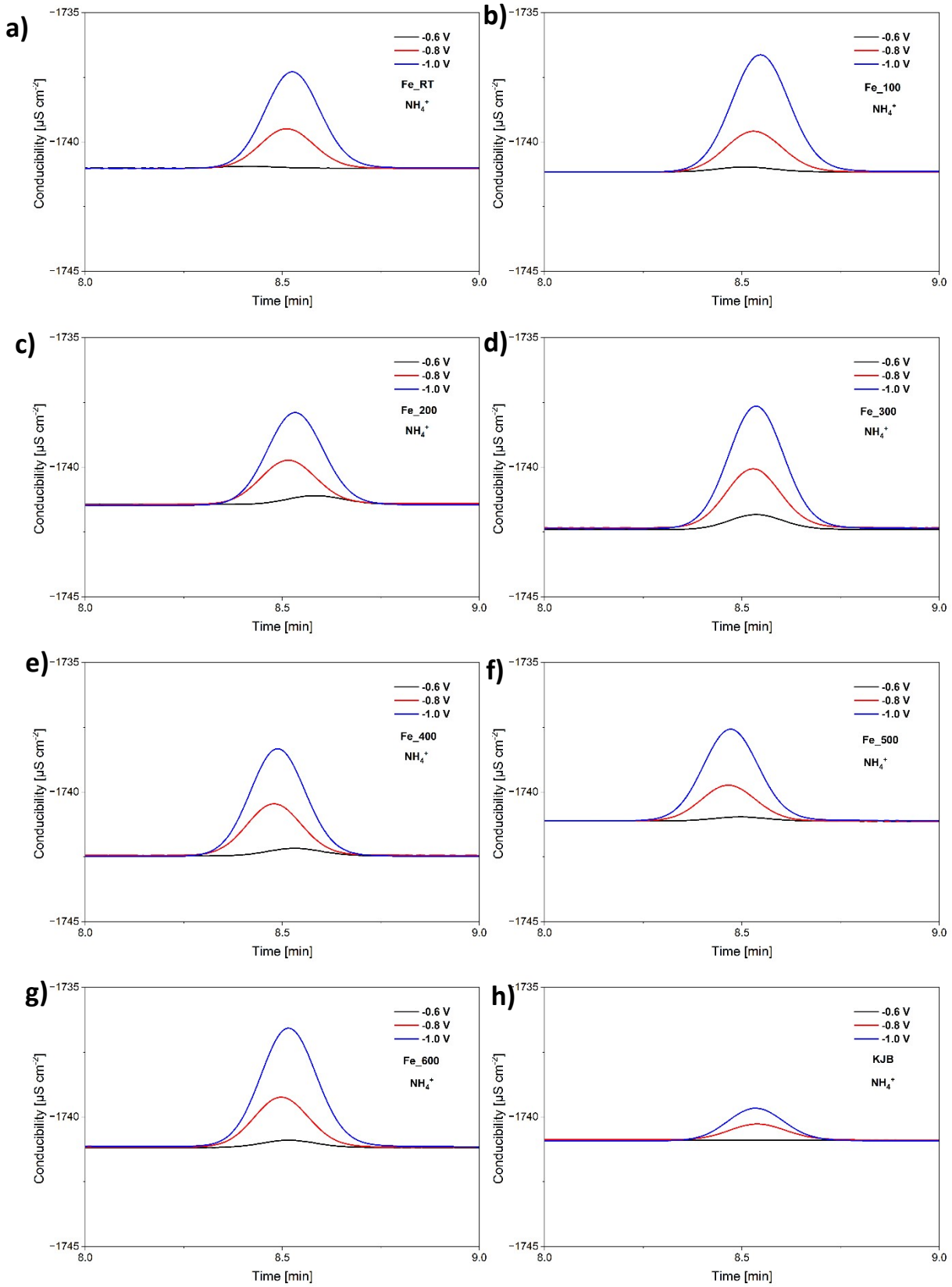

Figure S12. IC peaks for NH_4^+ detection in the catholyte (diluition 1:10) measured after each electrolysis over a) Fe_RT, b) Fe_100, c) Fe_200, d) Fe_300, e) Fe_400, f) Fe_500, g) Fe_600 and h) KJB. The samples were collected after CA performed at applied potentials of -1.0 V (blue), -0.8 V (red) and -0.6 V (black) vs. RHE, respectively.

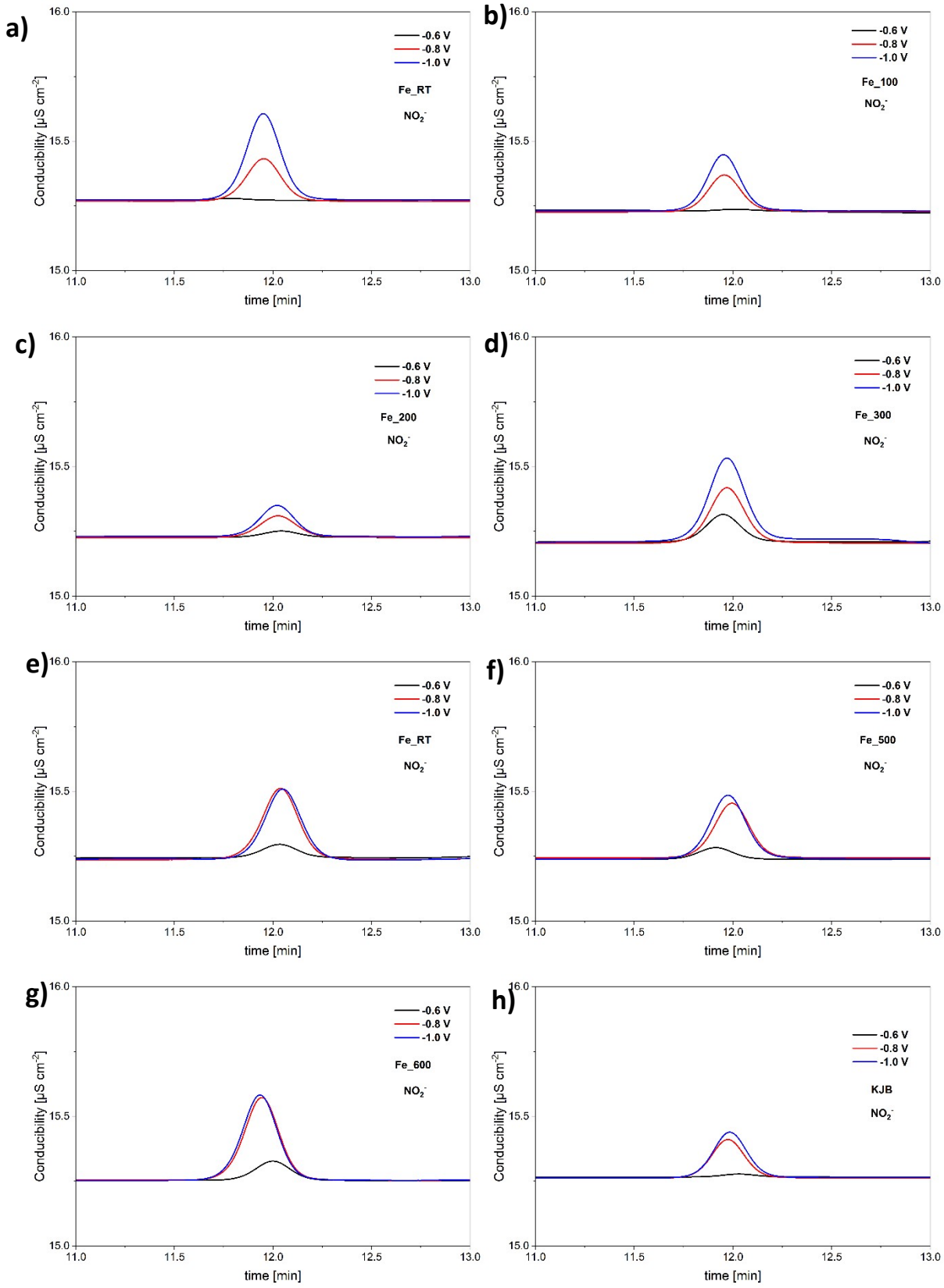

Figure S13. IC peaks for NO_2^- detection in the catholyte (diluition 1:50) measured after each electrolysis over a) Fe_RT, b) Fe_100, c) Fe_200, d) Fe_300, e) Fe_400, f) Fe_500, g) Fe_600 and h) KJB.The samples were collected after CA performed at applied potentials of -1.0 V (blue), -0.8 V (red) and -0.6 V (black) vs. RHE, respectively.

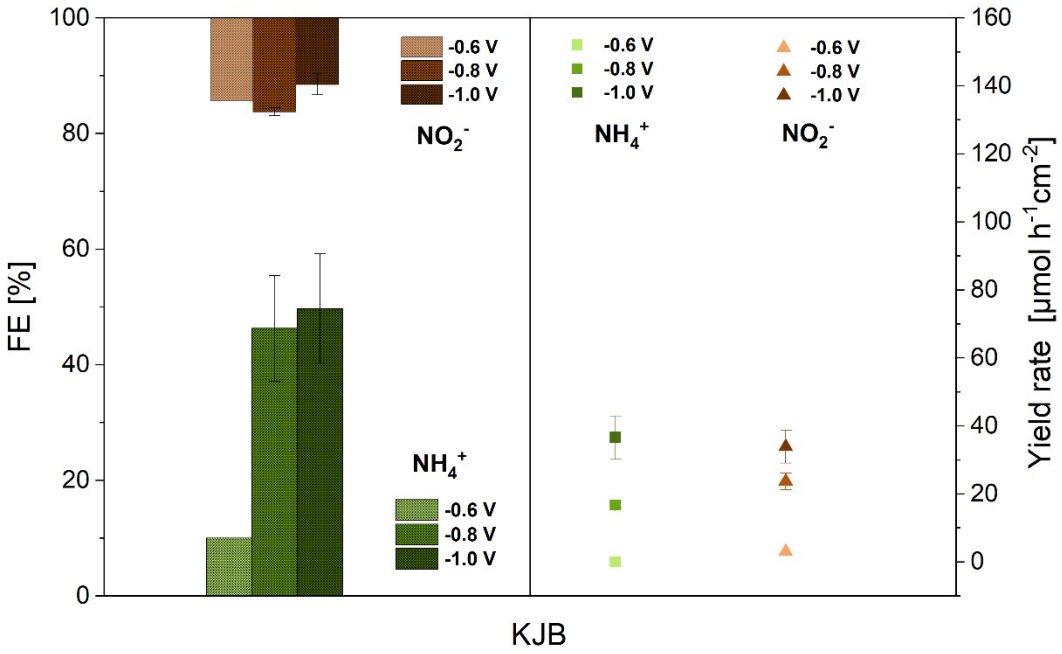

Figure S14. Activity and selectivity of the carbon support (KJB) for the electrochemical NO_3RR. On the left is reported the FE for NO_2^- (orange; top-down) and NH_4^+ (green; bottom-up) while on the right the yield rate for NO_2^- (orange; triangle) and NH_4^+ (green; square).

Table S6. FE and yield rate of NH_4^+ calculated for the carbon support (KJB) all ECs after 1h of CA in 0.1M PBS +0.16M NO_3^- at -0.6 V, -0.8 V and -1.0 V vs. RHE.

Sample	-0.6 V vs. RHE		-0,8 V vs. RHE		-1 V vs. RHE	
	FE (%)	yield rate (µmol h^{-1} cm^{-2})	FE (%)	yield rate (µmol h^{-1} cm^{-2})	FE (%)	yield rate (µmol h^{-1} cm^{-2})
KJB	0	0	46.29 ± 9.18	16.73 ± 0.86	49.7 ± 9.49	36.57 ± 6.41
Fe_rt	32.87 ± 10.24	3.04 ± 1.44	77.21 ± 2.02	44.45 ± 9.55	80.98 ± 0.55	96.03 ± 4.11
Fe_100	54.64 ± 0.36	4.2 ± 2.75	75.28 ± 3.73	43.09 ± 2.15	85.48 ± 6.65	104.93 ± 19.14
Fe_200	59.6 ± 7.33	8.66 ± 0.17	83.1 ± 0.65	41.72 ± 0.55	90.24 ± 3.31	96.03 ± 4.11
Fe_300	70.9 ± 5.24	12.27 ± 2.93	85.45 ± 2.37	57.58 ± 2.13	82.93 ± 2.26	123.69 ± 7.04
Fe_400	60.74 ± 2.83	7.22 ± 0.71	76.77 ± 4.03	51.34 ± 3.31	84.2 ± 1.84	120.5 ± 15.73
Fe_500	46.87 ± 4.74	5.48 ± 1.71	74.85 ± 6.47	35.22 ± 8.72	82.65 ± 0.43	89.5 ± 0.96
Fe_600	56.87 ± 2.28	6.32 ± 1.54	76.59 ± 0.70	44.67 ± 4.25	83.22 ± 1.14	116.06 ± 0.33

Table S7. FE and yield rate of NO_2^- calculated for the carbon support (KJB) and all ECs after 1h of CA in 0.1M PBS+0.16M NO_3^- at -0.6 V, -0.8 V and -1.0 V vs. RHE

Sample	-0.6 V vs. RHE		-0.8 V vs. RHE		-1.0 V vs. RHE	
	FE (%)	yield rate (µmol h^{-1} cm^{-2})	FE (%)	yield rate (µmol h^{-1} cm^{-2})	FE (%)	yield rate (µmol h^{-1} cm^{-2})
KJB	14.28	3.04	16.23 ± 0.72	23.74 ± 2.46	11.51 ± 1.80	33.89 ± 4.77
Fe_rt	7.89 ±0.36	2.82 ± 0.37	12.92 ± 3.78	28.80 ± 1.57	12.85 ± 0.46	60.98 ± 4.40
Fe_100	8.37 ± 2.86	2.69 ± 0.26	9.82 ± 1.61	22.48 ± 3.69	5.95 ± 1.57	29.48 ± 10.76
Fe_200	8.24 ± 2.70	4.72 ± 0.89	8.03 ± 0.38	16.13 ± 1.11	4.96 ± 0.96	20.33 ± 2.61
Fe_300	22.11 ± 0.91	15.59 ± 5.44	14.24 ± 0.53	38.37 ± 1.08	11.87 ± 2.24	71.48 ± 19.37
Fe_400	18.81 ± 2.40	8.96 ± 1.60	20.44 ± 0.67	54.74 ± 4.61	14.00 ± 3.10	81.54 ± 26.12
Fe_500	21.46 ± 6.67	9.59 ± 2.62	12.82 ± 6.19	24.14 ± 12.68	10.42	44.96
Fe_600	20.61 ± 9.05	9.78 ± 6.64	19.43 ± 4.30	45.87 ± 14.76	12.01 ± 2.00	67.07 ± 11.90

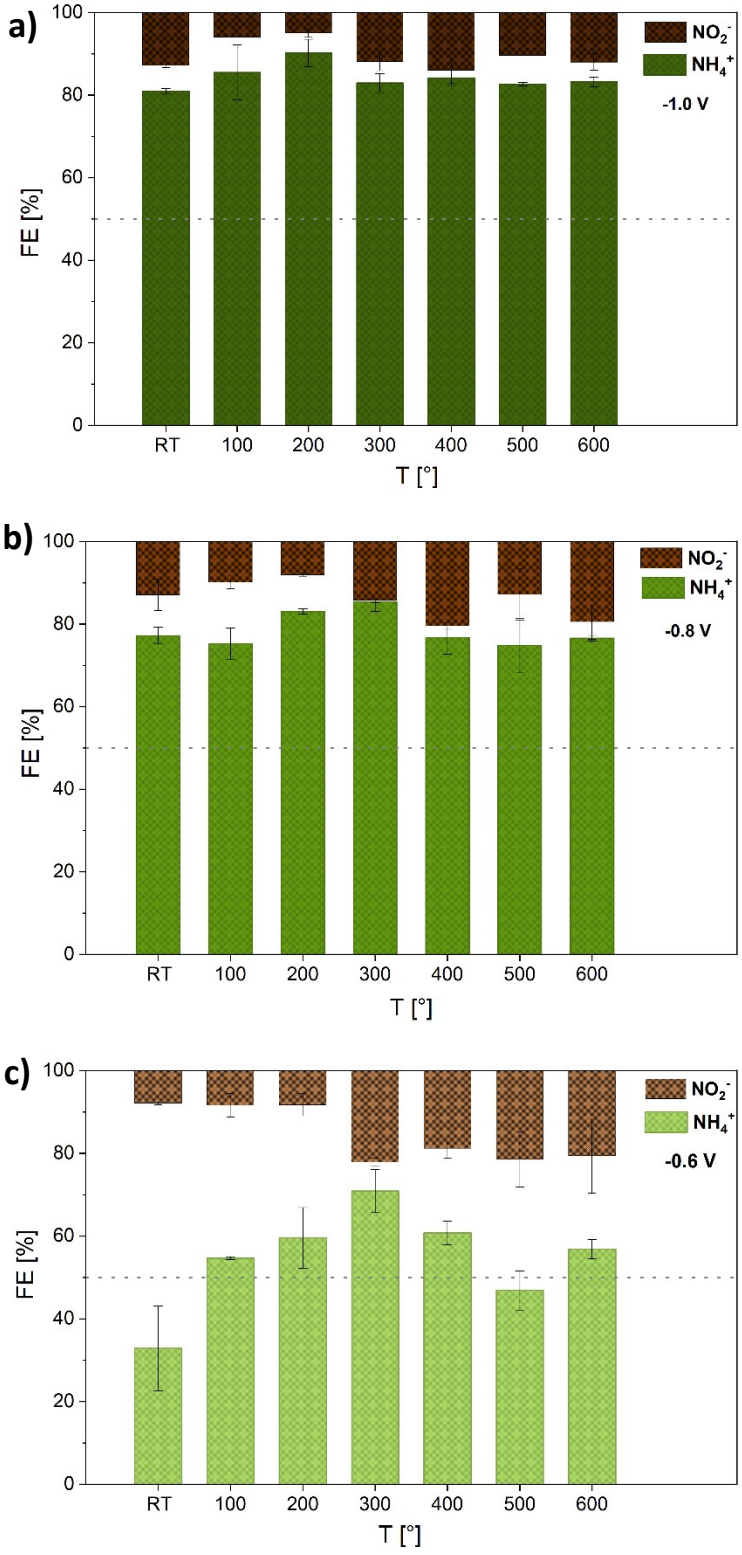

Figure S15. FE for NO_2^- (orange; top-down) and NH_4^+ (green; bottom-up) at a) -1.0 V, b) -0.8 V and c) -0.6 V vs. RHE for the electrochemical NO_3RR for all ECs in 0.1M PBS+0.16M NO_3^- for 1h. A horizontal line is set at 50% FE to guide the eye.

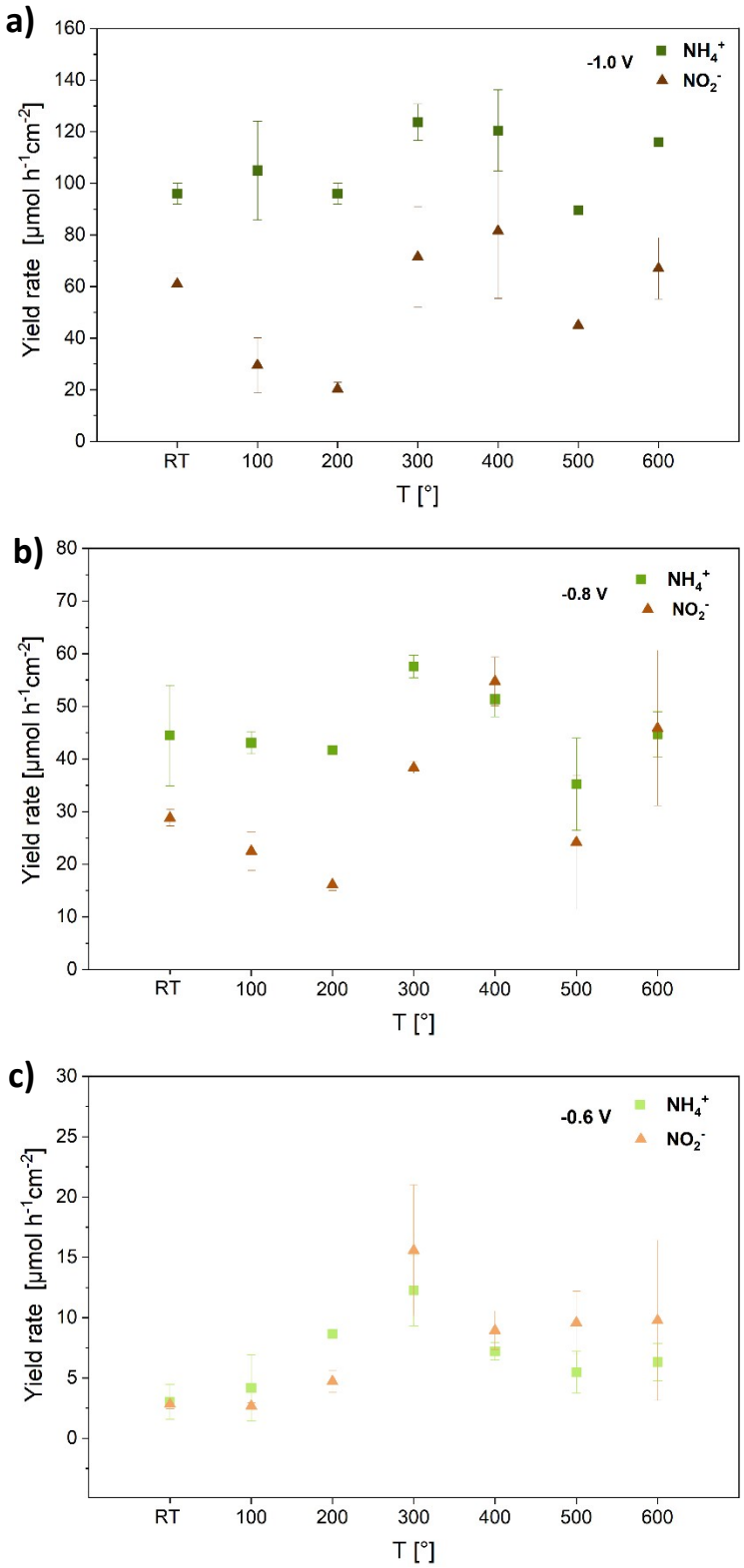

Figure S16. Yield rate for NO_2^- (orange; triangle) and NH_4^+ (green; square) at a) -1.0 V, b) -0.8 V and c) -0.6 V vs. RHE for the electrochemical NO_3RR for all ECs in 0.1M PBS+0.16M NO_3^- for 1h.

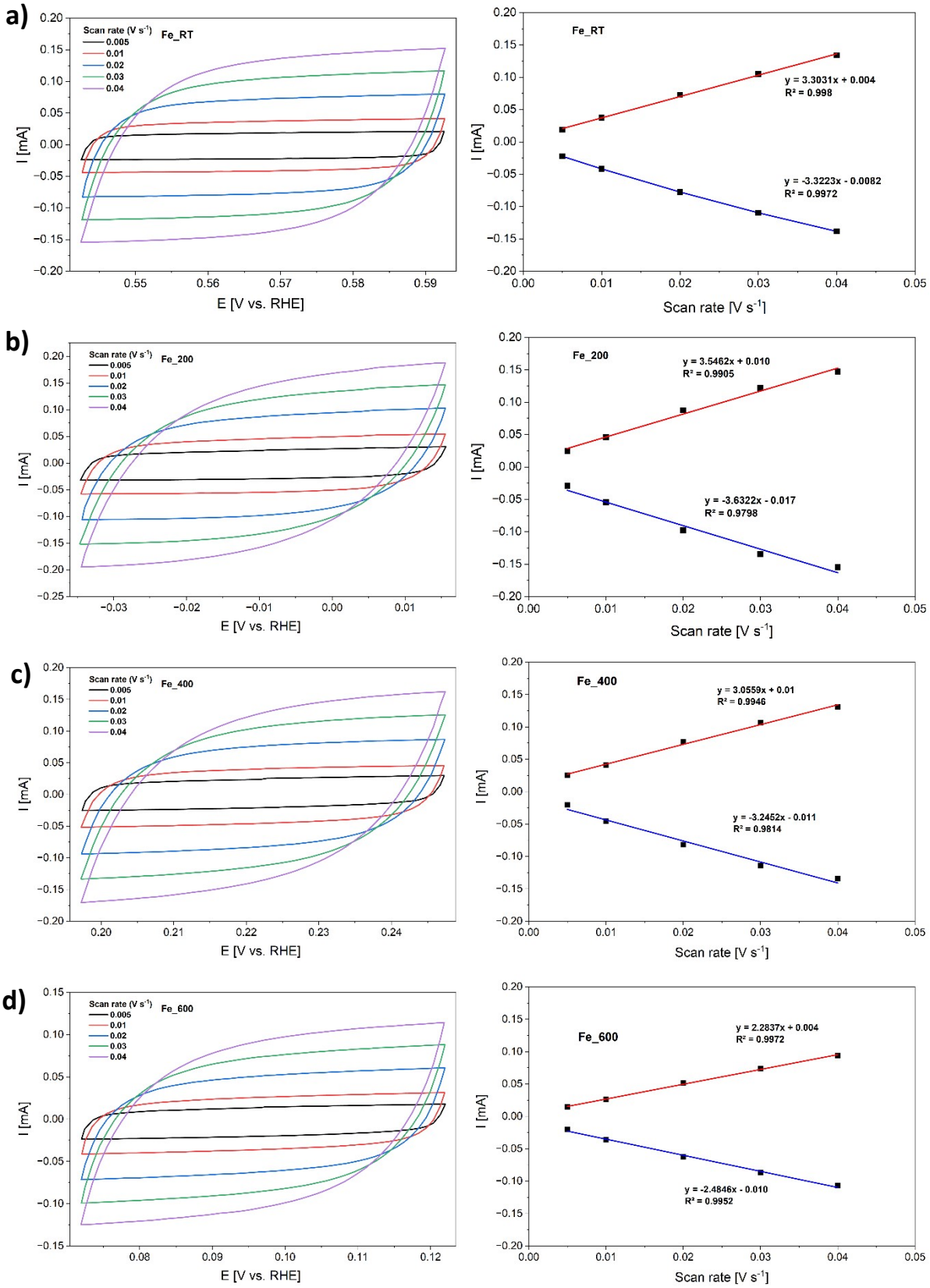

Figure S17. double-layer capacitance (Cdl) determination for a)Fe_RT, b) Fe_200, c) Fe_400 and d) Fe_600. On the left: cyclic voltammograms (CVs) recorded at different scan rates. On the right: current recorded at the OCP as a function of the the scan rate, where the red linear fit refers to the positive current at the OCP and the blue linear fin to the negative; the slopes of the linear fit were used for the calculation of Cdl.

Table S8. double-layer capacitance (Cdl) and electrochemical surface area (ECSA) calculated for each ECs

Sample	Cdl (mF)	ECSA (m^2g^{-1})
Fe_RT	3.31	84.51
Fe_200	3.59	89.73
Fe_400	3.15	78.76
Fe_600	2.38	59.60

Table S9**.** Comparison of the catalytic performance of different Fe-N_x-C EC for NO_3RR in previous works.

Catalyst	Overpotential (V vs. RHE)	Electrolyte	FE (%)	NH_3 Yield Rate (mmol h^{-1} cm^{-2})	Ref
Fe_300	**-0.8**	**PBS 0.1 M + 0.16 M NO_3^-**	**85.5**	**0.06**	**This Work**
Fe SAC (FeN_4)	-0.66	0.5 M KNO_3 + 0.1 M K_2SO_4	74.9	0.46	1
FeNx	-0.6	PBS 0.1 M + 0.16 M NO_3^-	~ 100%	0.01	2
Fe_{SAs}/g-C_3N_4	-0.65	0.1 M Na_2SO_4 + 50 mg N/L NO_3^--N	77.3	-	3
Fe-PPy SAC (FeN_4)	-0.4	0.1 M KOH + 0.1 M KNO_3	94.15	0.03	4
Fe_1/NC-900	-0.7	0.5 M KNO_3 + 0.1 M K_2SO_4	86	0.353	5
FeNCS	-0.57	0.02 M Na_2SO_4 + 5 mg $NaNO_3$	78.4	-	6
Fe SAC (FeN_2O_2)	-0.68	0.5 M KNO_3 + 0.1 M K_2SO_4	92	0.54	7

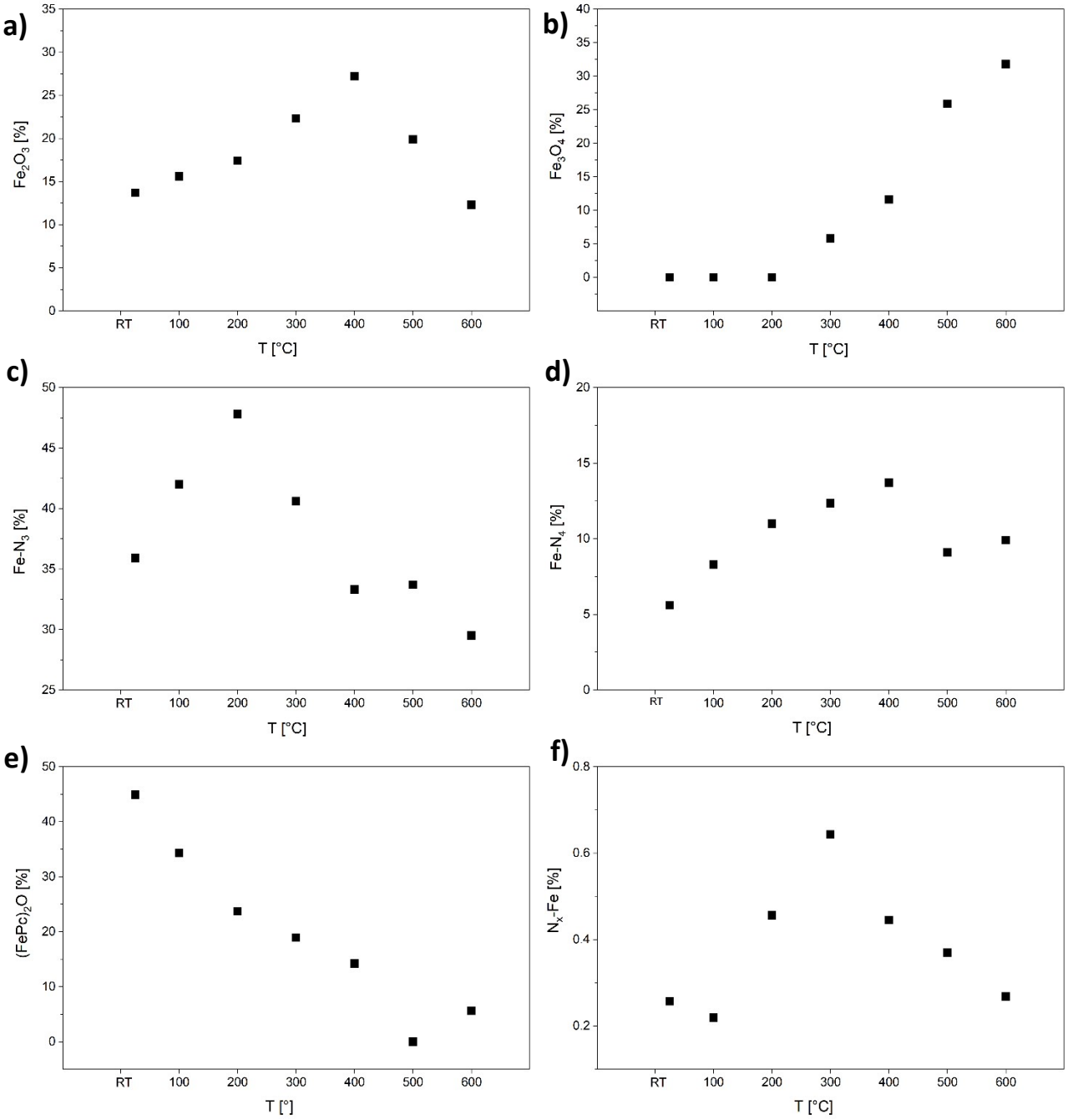

Figure S18. temperature-dependent evolution of each species. It has been considered the relative content of a) Fe_2O_3, b)Fe_3O_4, c) Fe-N_3, d) Fe-N_4, e) $(FePc)_2O$ obtained from XANES and the total f) N_x-Fe content derived from XPS N1s spectra.

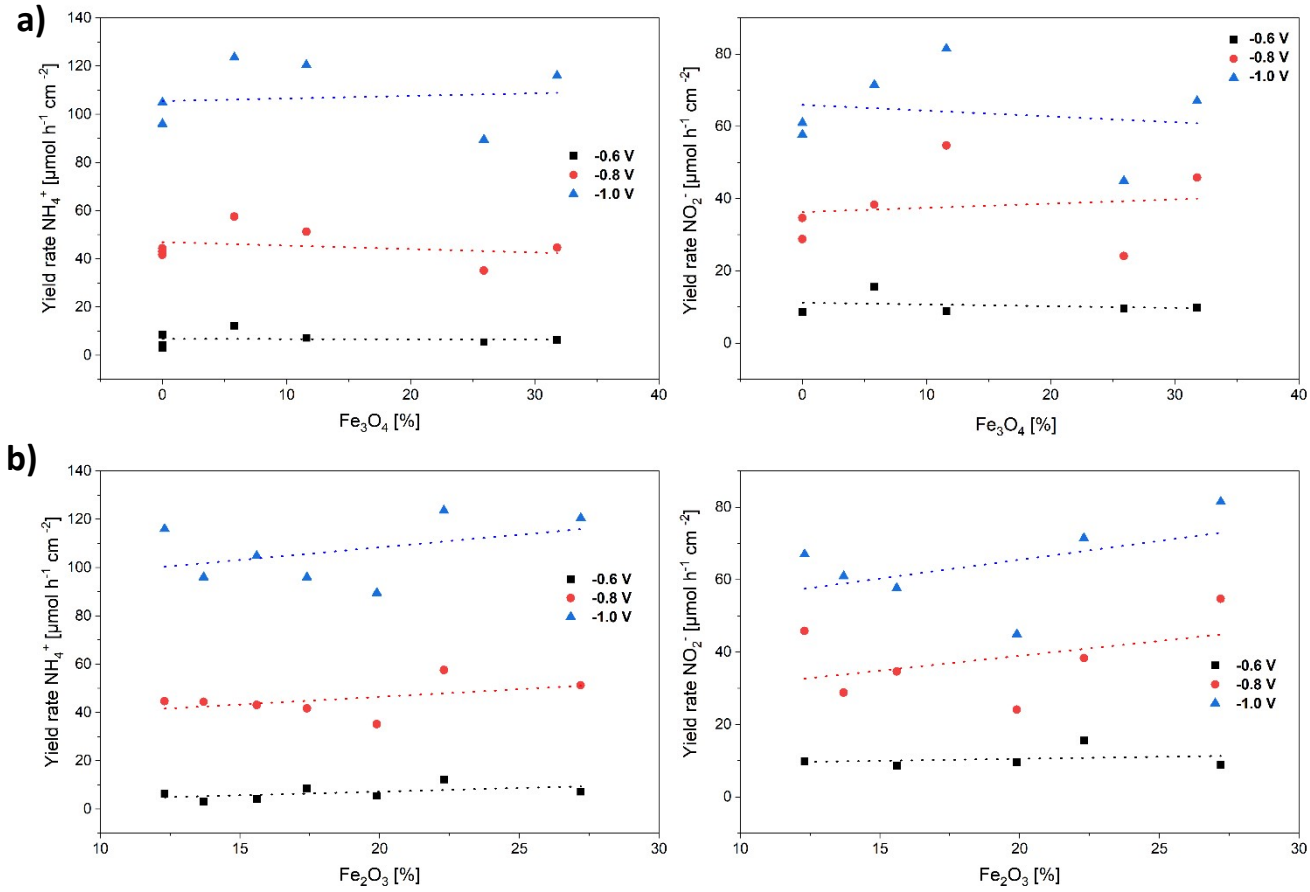

Figure S19. linear correlations between the yield rate and the relative content of a) Fe_3O_4 and b) Fe_2O_3, obtained from XANES. On the left is reported the plot vs NH_4^+ production while on the right vs NO_2^- production.

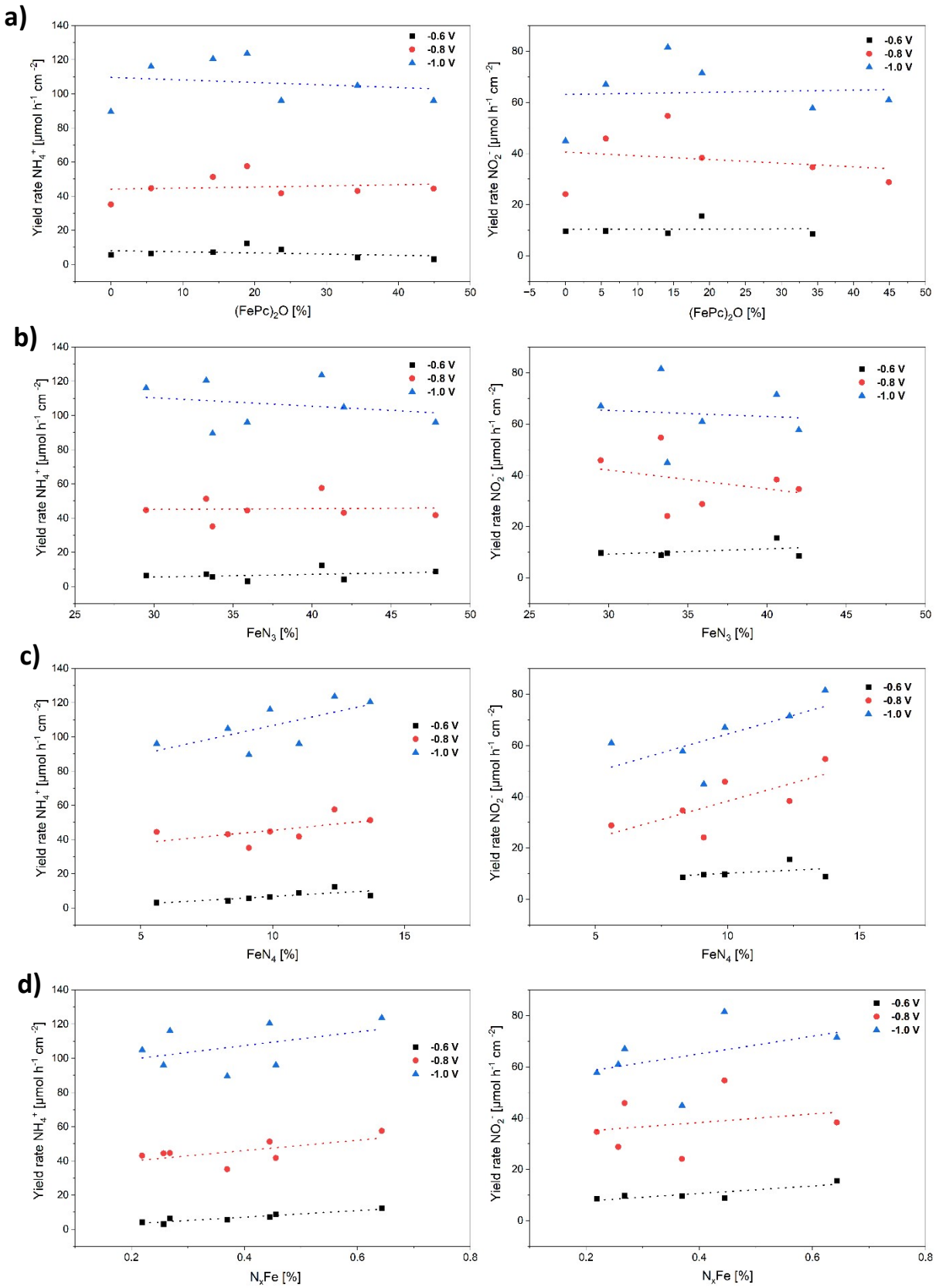

Figure S20. linear correlations between the yield rate and the relative amount of a) $(FePc)_2O$, b) FeN_3, c) FeN_4 obtained from XANES , and total amount of d) N_x-Fe derived from XPS N1s spectra. On the left is reported the plot vs NH_4^+ production while on the right the plot vs NO_2^- production.

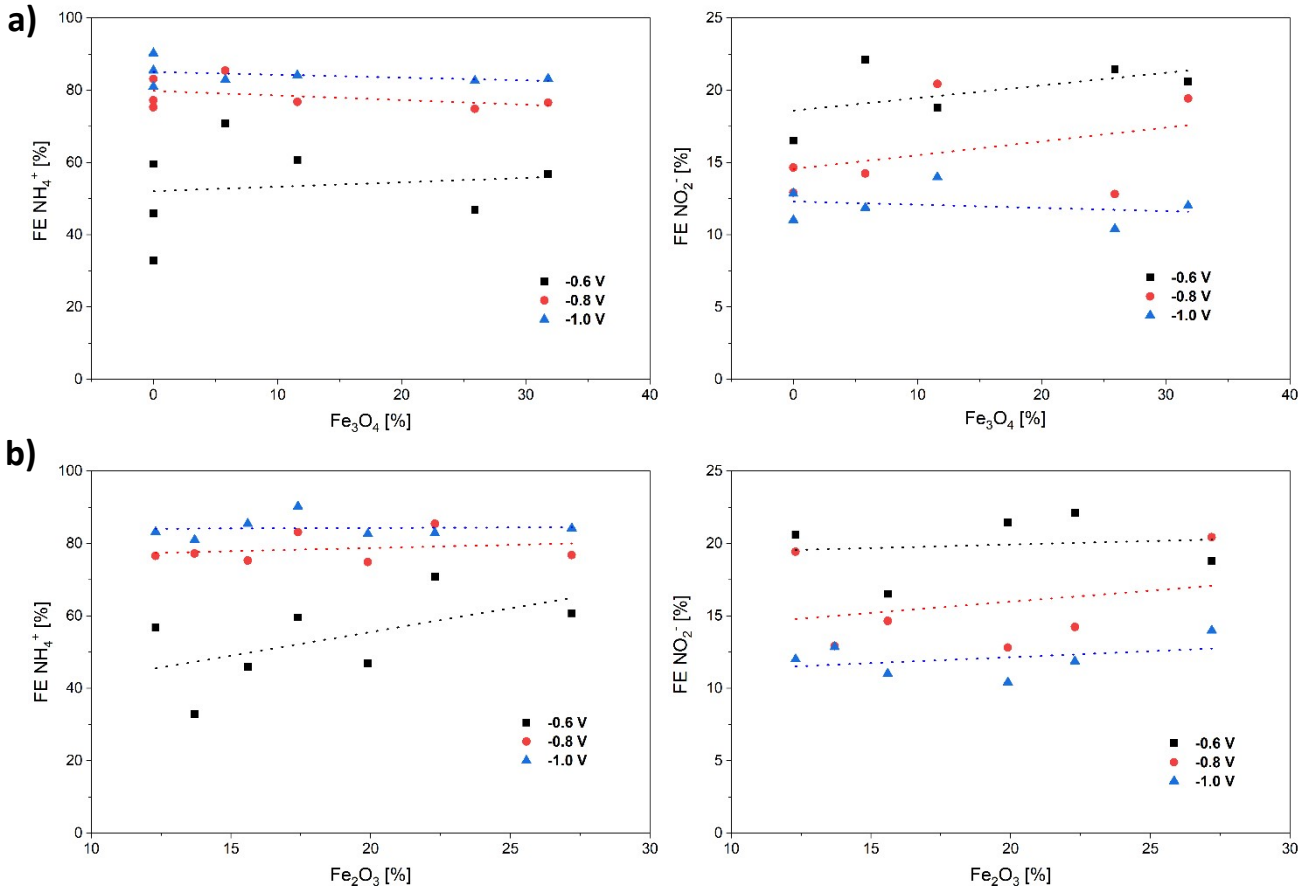

Figure S21. linear correlations between the FE and the relative abundance of a) Fe_3O_4 and b) Fe_2O_3. On the left is reported the plot vs NH_4^+ while on the right vs NO_2^-.

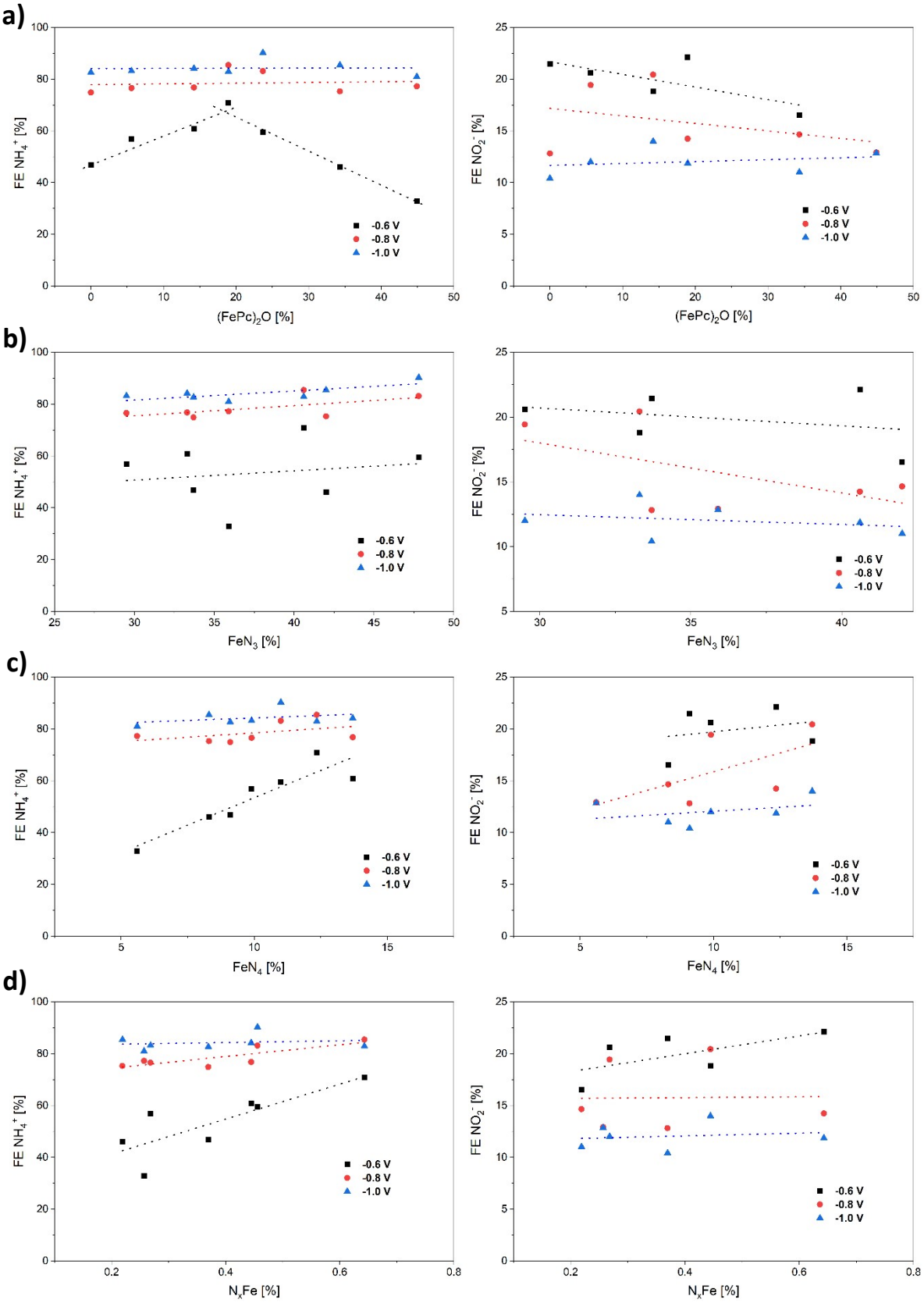

Figure S22. linear correlations between the FE and the relative amount of a) $(FePc)_2O$, b) FeN_3, c) FeN_4 derived from XANES and total amount of d) N_x-Fe derived from XPS N1s spectra. On the left is reported the plot vs NH_4^+ while on the right the plot vs NO_2^-.

Section S2: DFT calculations

Table S10. Entropic and zero-point energy contributions of all species at T = 298 K. The atoms in brackets represent those bound to the metal.

Species	TS /eV	E_{ZPE} /eV
$H_{2\,(g)}$	0.41	0.27
$H_2O_{\,(g)}$	0.58	0.56
$HNO_{3\,(g)}$	0.3	0.68
$NH_{3\,(g)}$	0.1	0.89
$NO_2(O)$*	0.39	0.42
$NO_2H(O)$*	0.5	0.72
$(N)O_2$*	0.25	0.3
$NO(O)$*	0.24	0.32
$(N)O_2H$*	0.35	0.58
$NO(O)H$*	0.35	0.59
$(N)O$*	0.12	0.17
$N(O)$*	0.11	0.19
$(N)OH$*	0.22	0.45
$NH(O)$*	0.19	0.48
$(N)HOH$*	0.14	0.77
$NH_2(O)$*	0.13	0.79
$(N)H_2OH$*	0.37	1.14
(N)*	0.03	0.07
(O)*	0.03	0.06
$(N)H$*	0.09	0.29
$(N)H_2$*	0.17	0.63
$(O)H$*	0.09	0.31
$(N)H_3$*	0.25	0.99
$H_2(O)$*	0.2	0.62

Table S11. Calculated Gibbs Free energies of most stable reaction intermediates adsorbed on FeN_4@Gr and FeN_3@Gr at $T = 298$ K and $V = 0$ V vs RHE.

FeN_4@Gr	**ΔG /eV**		**FeN_3@Gr**	**ΔG /eV**
$NO_2(O)*$	0.56		$NO_2(O)*$	-0.29
$NO_2H(O)*$	0.15		$NO_2H(O)*$	0.11
$(N)O_2*$	-1.4		$NO(O)*$	-1.95
$(N)O_2H*$	-1.51		$NO(O)H*$	-1.8
$(N)O*$	-3.09		$N(O)*$	-2.47
$(N)OH*$	-2.8		$NH(O)*$	-2.9
$(N)HOH*$	-3.02		$NH_2(O)*$	-3.83
$(N)H_2OH*$	-4.02		$(O)*$	-3.78
$(N)H_2*$	-5.43		$(O)H*$	-5.68
$(N)H_3*$	-6.86		$H_2(O)*$	-6.01

Table S12. Structural parameters of FeN_4@Gr and FeN_3@Gr catalysts: Fe-N(C) bond length and Fe magnetization (μ).

***d* /Å**	***FeN_4*@Gr**	***FeN_3*@Gr**
$Fe\text{-}N_1(C)$	*1.902*	*1.877*
$Fe\text{-}N_2$	*1.902*	*1.926*
$Fe\text{-}N_3$	*1.902*	*1.938*
$Fe\text{-}N_4$	*1.902*	*1.892*
μ(Fe)	*1.99*	*2.01*

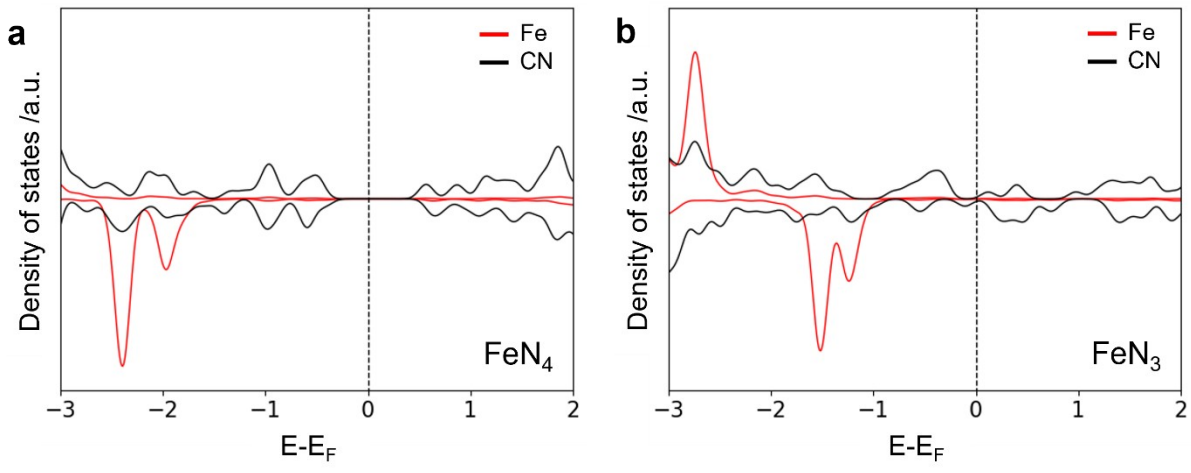

Figure S23. Projected density of states for (a) FeN_4 and (b) FeN_3.

Model structure of FeN_4@Gr:

1.000000000000000
9.8703498839999995 0.0000000000000000 0.0000000000000000
-4.9351760801999998 8.5479730867000008 0.0000000000000000
0.0000000000000000 0.0000000000000000 20.0000000000000000
C N Fe
26 4 1
Direct
0.0786509750422402 0.1624895702013794 0.0341639691416389
0.0828697917056540 0.4166197781091199 0.0345661592539097
0.0873549054041827 0.6689926531596768 0.0344141724072428
0.0827675319697073 0.9152467985316824 0.0340505783980524
0.3351953052277451 0.1765314439993760 0.0339657002602870
0.3255580692459852 0.4155097089585668 0.0342098745115238
0.3307808201173261 0.6689862735762153 0.0343855893107767
0.3371618504768291 0.9251854289001601 0.0341169468989729
0.5904658056986226 0.1765079538691313 0.0339879127979187
0.5816224061820481 0.9152543626216081 0.0340344569521560
0.8329738976422136 0.1624894038939499 0.0341943325168461
0.8391052614253354 0.4155174737355638 0.0342644943536050
0.8266897885752884 0.9042370582498462 0.0339877701317200
0.1663093067832316 0.0846224995472059 0.0340301200909630
0.1617268744639462 0.3308890002775694 0.0343740218769947
0.1662025045416865 0.5832571093495437 0.0345708712299218
0.1704273695936780 0.8373891330139152 0.0341813061269134
0.4223866311264451 0.0956409129970014 0.0339781285829105
0.4161029307753473 0.8373874214648956 0.0341795371667402
0.6674567830214462 0.0846226657560189 0.0340500755372556
0.6586112156693299 0.8233657668469119 0.0339642419823880
0.9119151000547441 0.0746936349428323 0.0341209434955941
0.9182930887790970 0.3308885780744192 0.0344121930768842
0.9235252945221361 0.5843694770173996 0.0342711596230930
0.9138815118080046 0.8233468005081305 0.0340024951601600
0.4099790042074494 0.5843615226401856 0.0342084524396422
0.5708755712095981 0.6601266670419458 0.0339202229036026
0.8383747134971897 0.6601133343519324 0.0339909864912851
0.4107088214636071 0.3397650937795990 0.0339435241262647
0.6782101538693673 0.3397465269904605 0.0339673813114390
0.6245526987351803 0.4999430842266211 0.0337767055433196

Model structure of FeN_3@Gr:

1.000000000000000
9.8703498839999995 0.0000000000000000 0.0000000000000000
-4.9351760801999998 8.5479730867000008 0.0000000000000000
0.0000000000000000 0.0000000000000000 20.0000000000000000
C N Fe
27 3 1
Direct
0.0792758119351551 0.1627947973857310 0.0341737900209355
0.0826834308784296 0.4167592867441628 0.0345792807715705
0.0861159096559648 0.6688538107175793 0.0343731407357231
0.0831902676135438 0.9158622881972710 0.0339772182459344
0.3350922155098601 0.1761080889242098 0.0339342858181627
0.3235717063549358 0.4136475857743327 0.0342189545901356
0.3301762498060333 0.6688336970905845 0.0343596785565353
0.3369079373622371 0.9250222904696778 0.0340840941405705
0.5908908093154456 0.1757788509321627 0.0340150273084023
0.5822729788545264 0.9155302404866548 0.0340162020820746
0.8329342286110848 0.1629990111520349 0.0342362114176229
0.8381315430552488 0.4149500063737526 0.0343047872794693
0.8296158687133232 0.9076762309155683 0.0339370805473381
0.1664120514011402 0.0845235216741145 0.0339853628819487
0.1609609962611779 0.3300028505902050 0.0343935333476348
0.1650346471128085 0.5831830340564120 0.0345452659797359
0.1704539302479878 0.8373988392706649 0.0341309412805023
0.4217593443361697 0.0947579413926370 0.0339532470542183
0.4165148133137166 0.8365778643263966 0.0341552773611307
0.6676746914790638 0.0841291197293016 0.0340694492697224
0.6610628606095238 0.8256532247448145 0.0339269703657089
0.9133430864112353 0.0755677321892044 0.0341291581834458
0.9180820044511742 0.3309308407707450 0.0344560631883651
0.9220857837005878 0.5845823343139300 0.0342583229965456
0.9149760767536447 0.8253002098834726 0.0339334361420261
0.4083505331395869 0.5823610722471824 0.0342094805854308
0.5727847452281383 0.6597531517475983 0.0339421749623754
0.8379475005804539 0.6617499635898949 0.0339812532144469
0.4092922145618471 0.3387666747088006 0.0339564836529805
0.6775506701950712 0.3364693882776564 0.0340608919848431
0.6255910753855464 0.5015731879561121 0.0339872597344856

References:

1 Z. Y. Wu, M. Karamad, X. Yong, et al., Electrochemical ammonia synthesis via nitrate reduction on Fe single atom catalyst, *Nat. Commun.,* 2021, **12**, 2870.

2 E. Murphy, Y. Liu, I. Matanović, et al., Elucidating electrochemical nitrate and nitrite reduction over atomically-dispersed transition metal sites, *Nat. Commun.,* 2023, **14**, 4843.

3 Q. Song, M. Li, X. Hou, et al., Anchored Fe atoms for N=O bond activation to boost electrocatalytic nitrate reduction at low concentrations, *Appl. Catal. B, 2022,* **317**, 121734.

4 P. Li, Z. Jin, Z. Fang, et al., A single-site iron catalyst with preoccupied active centers that achieves selective ammonia electrosynthesis from nitrate, *Energy Environ. Sci.* 2021, **14**, 3522–3531.

5 L. Liu, X. Zhao, H. Fu, et al., Construction and identification of highly active single-atom Fe1-NC catalytic site for electrocatalytic nitrate reduction, *Appl. Catal. B,* 2023, **323**, 122171

6 J. Li, M. Li, N. An, et al., Atomically dispersed Fe atoms anchored on S and N-codoped carbon for efficient electrochemical denitrification, *Proc. Natl. Acad. Sci. U.S.A*, 2021, **118**, 33e2105628118

7 W. Da Zhang, H. Dong, L. Zhou, et al., Fe-single atom catalysts with pre-organized coordination structure for efficient electrochemical nitrate reduction to ammonia, *Appl. Catal. B*, 2022, **317**, 121750.